

**İZMİR KATİP ÇELEBİ UNIVERSITY
GRADUATE SCHOOL OF NATURAL AND APPLIED SCIENCES**

**INVESTIGATION OF TUNABLE WETTING PROPERTIES OF MODIFIED
NATURAL MINERAL POWDERS**

M.Sc. THESIS

Hande ALPTEKİN

Department of Materials Science and Engineering

**Thesis Advisor: Asst.Prof.Dr. Mücahit SÜTÇÜ
Thesis Co-Advisor: Prof. Dr. Salih OKUR**

AUGUST 2015

**İZMİR KATİP ÇELEBİ UNIVERSITY
GRADUATE SCHOOL OF NATURAL AND APPLIED SCIENCES**

**INVESTIGATION OF TUNABLE WETTING PROPERTIES OF MODIFIED
NATURAL MINERAL POWDERS**

M.Sc. THESIS

**Hande ALPTEKİN
(Y130111034)**

Department of Materials Science and Engineering

**Thesis Advisor:Asst.Prof. Mücahit SÜTÇÜ
Thesis Co-Advisor:Prof. Dr. Salih OKUR**

AUGUST 2015

İZMİR KATİP ÇELEBİ ÜNİVERSİTESİ ★ FEN BİLİMLERİ ENSTİTÜSÜ

**MODİFİYE EDİLMİŞ DOĞAL MİNERAL TOZLARIN AYARLANABİLİR
ISLANMA ÖZELLİKLERİNİN İNCELENMESİ**

YÜKSEK LİSANS TEZİ

**Hande ALPTEKİN
(Y130111034)**

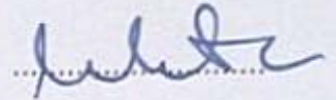
Malzeme Bilimi ve Mühendisliği Anabilim Dalı

**Tez Danışmanı: Yrd.Doç.Dr. Mücahit SÜTÇÜ
Tez Eş Danışmanı: Prof.Dr. Salih OKUR**

AĞUSTOS 2015

Hande Alptekin, a M.Sc. student of İzmir Katip Çelebi University student ID Y130111034, successfully defended the thesis entitled "Investigation of tunable wetting properties of modified natural mineral powders", which she prepared after fulfilling the requirements specified in the associated legislations, before the jury whose signatures are below.

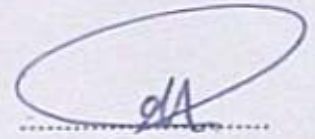
Thesis Advisor: Asst.Prof.Dr.Mücahit SÜTÇÜ
İzmir Katip Çelebi University



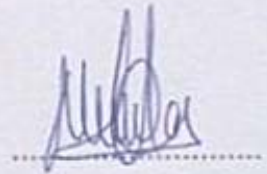
Thesis Co-Advisor: Prof. Dr. Salih OKUR
İzmir Katip Çelebi University



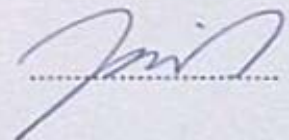
Jury Members: Asst.Prof.Dr.M.Hadi ZAREIE
İzmir Institute of Technology



Asst.Prof.Dr. Mustafa CAN
İzmir Katip Çelebi University



Asst.Prof.Dr.Nesrin HORZUM POLAT
İzmir Katip Çelebi University



Date of Submission: 12 August 2015
Date of Defense : 20 August 2015

To my family,

ACKNOWLEDGEMENT

Firstly, I want to state my gratitude to my advisor Asst.Prof.Dr. M¼cahit S¼T¼Ç¼ for the continuous support of my study and related research, for his understanding, immense knowledge and motivation. His direction helped me in all the time of research and composing of this thesis. I could not have imagined having a better advisor and mentor for my master thesis.

I am very thankful to İzmir Kâtip Çelebi University, Coordinator of BAP (Project number: 2013-2-FMBP-46) for their financial support and I am also grateful to my co-advisor Prof.Dr. Salih OKUR for spending time reading this thesis and for his guidance and support for research and providing useful suggestions and ideas about my thesis.

Besides my advisors, my sincere thanks also goes to Asst.Prof.Dr. Mustafa Can who gave me a chance to join his group, and who gave access to the laboratory and research facilities. Without his valuable support it would not be feasible to handle this research.

I would like to thank Research Assistant Emre Arkan, for his indulgent comments and encouragement, also thankful to for his directive recommendation for my entire thesis.

I am very grateful to all the people I have met along the way and contributed to the development of my research.

Last but not the least, I would like to thank my family: my parents and to my brother for supporting me profoundly all through composing this thesis and my life in general.

August 2015

Hande ALPTEKİN

TABLE OF CONTENTS

	<u>Page</u>
ACKNOWLEDGEMENT	ix
TABLE OF CONTENTS	xi
ABBREVIATIONS	xii
LIST OF FIGURES	xvii
SUMMARY	xix
ÖZET	xxi
1. INTRODUCTION	1
1.1. Hydrophobicity And Superhydrophobicity	1
1.2. Application Areas of Superhydrophobic Surfaces	2
2. THEORY	4
2.1. Contact Angle and Young's Equation	4
2.2. Surface Roughness	5
3. NATURAL MINERALS	8
3.1. Diatomaceous Earth	8
3.2. Talc	10
4. SILANE MODIFICATION	12
4.1. Formation of Silane Monolayers	12
5. MATERIALS AND METHOD	15
5.1. Materials	15
5.2. Synthesis of Superhydrophobic Diatomaceous Earth	17
5.3. Characterization Methods	18
5.3.1. Particle size and surface area (Brunauer-Emmett-Teller) analysis	18
5.3.2. FESEM (Field Emission Scanning Electron Microscopy) analysis	19
5.3.3. XRF (X-ray fluorescence Spectrometer) analysis	19
5.3.4. XPS (X-ray Photoelectron Spectrometer) analysis	19
5.3.5. TGA (Thermogravimetric analysis)	19
5.3.6. Contact Angle Analysis	19
5.3.7. Water Vapor Affinity Measurements	20
6. RESULT AND DISCUSSION	21
6.1. XRF, XRD, BET, Particle Size and SEM Analysis of As-received and Calcined DE Minerals	21
6.2. Water Vapor Affinity Results	25
6.3. TGA, BET, XPS and Contact Angle Analysis of Modified DE Samples	27
6.4. Advancing and Receding Contact Angles Results	31
6.5. Effects of Different Silane structures and Degree of Functionality	33
6.6. Talc Mineral Results	35
7. CONCLUSION	39
7.1. Recommendations for Future Works	40
8. REFERENCES	41
CURRICULUM VITAE	46

ABBREVIATIONS

SH	: Superhydrophobic
CA	: Contact Angle
DE	: Diatomaceous Earth
Mg₃Si₄O₁₀(OH)₂	: Hydrous Magnesium Silicate
SAM	: Self Assembled Monolayers
RH	: Relative Humidity
SiO₂	: Silicondioxide
N₂	: Nitrogen
R₀	: Initial Resistance
ΔR	: Change in the resistance
CAH	: Contact angle hysteresis
SA	: Sliding Angle
OTFE	: Oligomeric Tetrafluoroethylene
Mtcos-MCS	: 11-(chlorodimethylsilylmethyl)tricosane
Deca-BisTCS	: 1,2-Bis(trichlorosilyl)decane
Ethyl-MCS	: Ethyldimethylchlorosilane
nBut-MCS	: n-butyldimethylchlorosilane
Dodec-MCS	: Dodecyldimethylchlorosilane
FHex-MCS	: Nonafluorohexyldimethylchlorosilane
PFOct-MCS	: Dimethylchlorosilaneperfluorooctyl
PFDec-MCS	: Perfluorodecyl-1H,1H,2H,2H-dimethylchlorosilane

LIST OF TABLES

	<u>Page</u>
Table 1: Hydrophobicity and the Contact Angle	3
Table 2: Summary of Surface Functionalized Minerals	18
Table 3: Chemical Composition Analysis of “As-received” Sample (wt.%).....	21
Table 4: Effect of Calcination of DE on Chemical Composition , Surface Area and Partical Size Analysis (wt.%)	24
Table 5: Influence of Reaction Parameters on Key Features of Treated DE Samples.....	27
Table 6: Chemical Composition and BET Analysis of “As received” Talc (wt.%)	35
Table 7: Particle size analysis of the as-received talc.....	36

LIST OF FIGURES

	<u>Page</u>
Figure 1.1: Lotus leaf	1
Figure 1.2: Hydrophobicity and Superhydrophobicity	2
Figure 2.1: Representation of the CA	5
Figure 2.2: Illustration of Advancing and Receding Contact Angles	5
Figure 2.3: Wetting of Rough Hydrophobic Surfaces	6
Figure 3.1: Skeleton Symmetries of Diatoms	8
Figure 3.2: SEM micrograph of diatomit.....	9
Figure 3.3: Talc Structure	10
Figure 3.4: Electron Microscope Image of Talc Particle	11
Figure 4.1: Reaction of Silanes with Hydroxilated Surfaces	13
Figure 5.1: Silane Modifiers Used	16
Figure 6.1: The XRD Patterns of the As-received DE.....	22
Figure 6.2: The XRD Patterns of the Calcined DE.....	23
Figure 6.3: TGA Curves of As-received Diatomite.....	24
Figure 6.4: SEM micrographs of a) “As-received” DE, b) Calcined DE at 400°C	25
Figure 6.5: Effect of Grafting Density on Water Vapor Affinity of Samples	27
Figure 6.6: TGA Thermograms of PFOct-MCS grafted samples, b) Effect of PFOct-MCS grafting Density on TGA Weight Loss	28
Figure 6.7: Effect of Grafting Density on Average Static Contact Angle	29
Figure 6.8: XPS Survey Spectrums of a) HME-Blank, b) HME-4.....	30
Figure 6.9: Shape of Water Droplets Illustrating Wetting Behavior of HME-4 a) Inclined Surface for Advancing and Receding Contact Angles, b) 10 μ l of Water Droplet Pinned to the Surface of HME-4, c) Water Droplet Extended to 5 μ l for Advancing Contact Angle, d) Water Droplet Contracted to 4 μ l for Receding Contact Angle.....	32
Figure 6.10: Shape of Water Droplets Illustrating Wetting Behavior of HME-3 a) Water Droplet Extended to 5 μ l for Advancing Contact Angle, b) Water Droplet Contracted to 4 μ l for Receding Contact Angle.....	33
Figure 6.11: Changes in Water Contact Angle with regards to Different Silane Structures a) PFDec- MCS Modified DE (HME-4), b) PFOct-MCS Modified DE (HME-6), c) FHex-MCS Modified DE (HME-7), d) Dodec-MCS Modified DE (HME-10), e) nBut-MCS Modified DE (HME-8), f) Ethyl-MCS Modified DE (HME-9).....	34
Figure 6.12: a) Effect of Chain Variation on Water Contact Angle (HME-9), b) Effect of Degree of Functionality on Water Contact Angle (HME-12)	35
Figure 6.13: TGA Curves of As-received Talc.....	36
Figure 6.14: The SEM Images of the As-received Talc	37
Figure 6.15: The XRD Patterns of the 400°C Calcined Talc.....	37
Figure 6.16: Water Contact Angles of PFDec-MCS Modified TALC a) HME-13, b) HME-14.....	38
Figure 6.17: Dynamic Contact Angle Measurement of HME-14.....	38

INVESTIGATION OF TUNABLE WETTING PROPERTIES OF MODIFIED NATURAL MINERAL POWDERS

SUMMARY

In this thesis a feasible methodology was presented to prepare non wetting surfaces from natural mineral powders (diatomaceous earth and talc). Various ranges of silanes were used for the surface grafting and the best customization was achieved by monochlorosilane. Water affinity analysis of surface functionalized diatomaceous earth was the key aspect of loading tunable wettability on particle surface. Covalent attachment was confirmed via X-ray photoelectron spectroscopy (XPS), while thermogravimetric analysis, nitrogen adsorption isotherms, and contact angle measurements were used for the evaluation of grafting density and other fundamental features of hydrophobic particles. Diatomaceous earth was chosen as a prototype to develop efficient strategy for surface modification which can be applied to another natural particle so-called talc that represents dichotomic performance to water. The present study paved the way for a new approach that can be employed to any proper inherent texture for the production of superhydrophobic powders.

MODİFİYE EDİLMİŞ DOĞAL MİNERAL TOZLARIN AYARLANABİLİR ISLANMA ÖZELLİKLERİNİN İNCELENMESİ

ÖZET

Bu tezde doğal mineral tozlarından (diatomit ve talk) su tutmayan yüzeylerin hazırlanması için uygulanabilir yöntemler sunulmuştur. Yüzey aşılması için farklı silan çeşitleri kullanılmış ve en iyi sonuç mono klorosilan ile alınmıştır. Yüzey modifikasyonu yapılmış diatomitlerin su hassasiyet analizleri, parçacık yüzeyi üzerindeki ayarlanabilir ıslanma özelliklerinin incelenmesi için önemli bir çalışmadır. Mineral toz üzerine yapılan aşılama sonrasında yüzeydeki kovalent bağlanma X-ışını fotoelektron spektroskopisi (XPS) ile teyit edilmiştir. Termogravimetrik analiz, azot adsorpsiyon izotermeleri ve temas açısı ölçümleri, aşılama yoğunluğu ve hidrofobik partiküllerin diğer temel özelliklerinin değerlendirilmesinde kullanılmıştır. Diatomit minerali yüzey modifikasyonunda etkili bir strateji geliştirmek için prototip olarak seçilmiş ve yapılan çalışmalar suya karşı iki yönlü davranışta bulunan diğer bir doğal mineral olan talk üzerine uygulanmıştır. Bu tez çalışması uygun doğal minerallerden süperhidrofobik tozların üretilmesi için yeni bir yaklaşıma yol gösterici olmuştur.

1. INTRODUCTION

The thought of getting to know observing and comprehending new concepts from nature for the copy of appealing biological characteristic is called biomimetics. They has recently been getting a lot of attention with scientist for advanced materials [1]. These appealing biological characteristic are made by the agency of exquisitely designed surfaces or interfaces including structural properties on the micro or nano-scale. Observation of these tiny features is now possible with developments in characterization techniques such as electron microscopy allowing for a greater understanding of their mechanisms.

1.1. Hydrophobicity and Superhydrophobicity

Since the 1990's researchers have thoroughly studied on superhydrophobic and self-cleaning leaf surfaces; the lotus leaf isthe most well known and it is first to be investigated in great detail, as shown in Figure 1.1 [2-4]. In many scientific studies nature has been inspiration for humans as in this regard. The development of hydrophobic materials been inspired from the lotus leaf. They has been getting a lot of interest with scientists for developed materials.

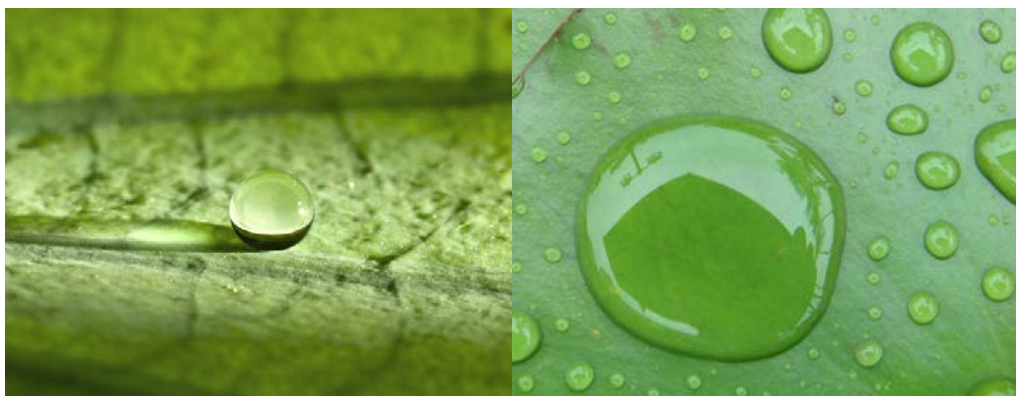


Figure 1.1: Lotus Leaf [URL-1]

Hydrophobic means water fearing or water repelling. Hydrophilic means basically water loving. These words can be explained in terms of contact angle is measure of static hydrophobicity. If contact angle of water droplet on the surface is larger than 90° , called hydrophobic. If contact angle of water droplet on the surface is smaller than 90° , called hydrophilic. Difference between hydrophobic and superhydrophobic surface can be also defined with contact angle. As previously mentioned above ,the basic explanation of hydrophobicity is a surface having a static water contact angle higher than 90° called hydrophobic and, while a superhydrophobic surface should display a contact angle higher than 150° , as shown in Figure 1.2.

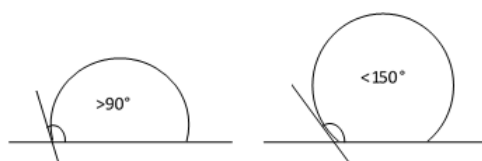


Figure 1.2: Hydrophobicity and Superhydrophobicity


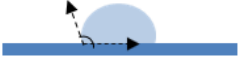
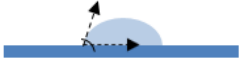

A surface can be changed to adjust its wettability. The two fundamental variables that can produce such changes are roughness of the surface and chemical composition. Desired water repellency can be attributable to strict regulation of key parameters that can repel the water and liquids even with remarkably lower surface energy values as in the case of many alcohols and alkanes [5]. Techniques to attain appropriate superhydrophobicity comprises wax solidification, lithography, polymer reformation, layer-by-layer methods, electrospinning, spraying, particle impregnation and fluorinated polymers or long hydrocarbon chains as surface grafting articles [5, 6]. Such organic modifiers not only display increased hydrophobicity through driving low surface energy but also they can be impregnated to the surface of inherent structure such as natural minerals and textiles [5-11]. However, there have been no controlled studies which can be feasible as well as cost-effective to produce durable nonwetting surfaces from unprocessed and “as-received” natural particles.

1.2. Application Areas of Superhydrophobic Surfaces

In recent years, low-cost and highly efficient superhydrophobic (SH) natural particles have attracted much attention for both principal and practical terms because of its

unique characteristic properties such as self-cleaning, antifouling, anti-adhesion and the rapid progress about their contributions to surface energy and nonpareil ability to repel water [12-16]. Superhydrophobic and self-cleaning surfaces have important act in technical applications, which can be protection towards marine fouling, microfluidics, lab-on-chip devices, self-cleaning paints, ice prevention and textiles. Reversible superhydrophobicity is the important application of superhydrophobic surfaces is, that is the capability of a surface to exchange between the hydrophobic and hydrophilic position. It means that surface change its hydrophobic or hydrophilic features under the influence of electrical potential, UV or light irradiation o temperature. Their reversible surface was employed in DNA nano devices. The self cleaning effect is particularly important for optical applications such as solar panels, lenses and mirrors, that have to stay clean [17].

Table 1: Hydrophobicity and the Contact Angle

Surface	Contact Angle	Figure
Superhydrophobic	>160	
Hydrophobic	>90	
Hydrophilic	<90	
Superhydrophilic	~ 0	

2. THEORY

2.1. Contact Angle and Young's Equation

The state of a fluid bead is dictated by the surface tension of the fluid. In an immaculate fluid, every molecule in the mass is pulled just as in every bearing by neighboring fluid particles, bringing about a net power of zero. Not with standing, the molecules uncovered at the surface don't have neighboring particles in all bearings to ensure a balanced net force. In lieu, the neighboring molecules pulled them inwards, creating an internal pressure. Accordingly, the liquid intentionally gets its surface area to keep up the most minimal surface free energy. This intermolecular force to get the surface is known as the surface tension, and it is dependable for the shape of liquid beads. Therefore, the contact angle is identified by a combination of surface tension and external forces. All liquid have surface energy. A surface can be thought as the interface between two phases. There are also surface energy between liquid and vapor ,solid and liquid and solid and vapor. The contact angle can described as the angle shaped by the intersection of the liquid-solid interface and the liquid-vapor interface. Where solid, liquid, and vapor co-exist, the interface is described as the "three phase contact line". The contact angle (CA) is related to the three interfacial surface tensions through the Young's equation. (equation 2.1)

If the liquid extends over the surface, a small contact angle is observed, otherwise the liquid beads over the surface, contact angle is observed large. Contact angle less than 90° shows that surface permits wetting while contact angles greater than 90° indicates that wetting of the surface is unsuitable that cause the fluid reduce its contact with the surface and shape a compact liquid droplet. Surfaces like these called as "hydrophobic surfaces". Additionally, superhydrophobic surfaces generally have a low surface energy with a contact angle (CA) greater than 150° at room temperatures (about 25°C) and bind very weakly with drops of water that results in formation of water beads [13, 18]. If contact angles are greater than 150° , showing nearly no contact between the liquid droplet and the surface demonstrates the lotus

effect. Therefore, the spreading of a liquid on a structured surface is generally expressed with a Young's equation using interfacial free energy functions of three boundaries that are in turn solid-liquid-vapor[19, 20].

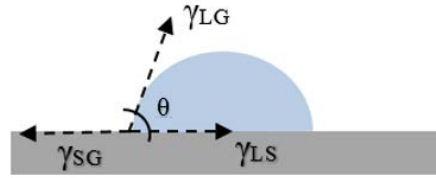


Figure 2.1: Representation of the CA

Thomas Young [21] described in 1805, a liquid drop the contact angle on an ideal solid surface is characterized by the mechanical equilibrium of the drop under the activity of three interfacial tensions (Figure 2.1). Force balance in the x direction is done for obtaining contact angle that is related to the three interfacial surface tensions through the Young's equation:

$$\gamma_{lg} \cos \theta_Y = \gamma_{sg} - \gamma_{sl} \quad (2.1)$$

where γ_{lg} , γ_{sg} and γ_{sl} represent the liquid-gas, solid-gas, and solid-liquid interfacial tensions, respectively, and θ_Y is the contact angle. Equation (2.1) is referred to as Young's equation [22].

1.3. Surface Roughness

Surface roughness extremely influence the surface wetting character. Topographic defects and modify the surface roughness can be obtained by methods like etching, crystal growth and nanolithography [13]. Such structures can copy fascinating natural frameworks in view of hydrophobicity, for example, the legs of the water strider then again self-cleaning of lotus leaves.[23, 24]

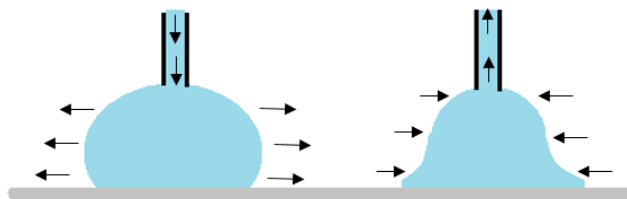


Figure 2.2: Illustration of Advancing and Receding Contact Angles

Young's equation is a very simplistic approximation that can be used only with ideally flat surfaces [22]. Real surfaces often do not follow Young's equation and present a range of CA values. Due to the surface inhomogeneity the contact line between three interfaces can experience various metastable states having diverse contact angles [25]. The measurable macroscopic CA can vary between the maximum value, called the advancing CA (θ_a) and the minimum value called the receding CA (θ_r) (Figure 2.2). The two can be measured utilizing a moving drop on a tilted surface as the front and the back angle, respectively. On the other hand, θ_a appears as a stabilized CA during addition of liquid to a drop. In the same way, during the removal of liquid from a drop the CA stabilizes at θ_r . Hysteresis is called as difference between θ_a and θ_r . θ_Y lies between θ_a and θ_r .

$$H = \theta_a - \theta_r \quad (2.2)$$

The rough surface divided in two categories: homogeneous or heterogeneous. In homogeneous wetting regime liquid fills in the roughness grooves of a surface. A heterogeneous wetting regime surface includes two types of patches. A significant model of such a composite surface is one composed of patches of both air and solid. Such surfaces have varied effects on the contact angles of wetting liquids [26]. There are two main models accessible describing wetting of a rough hydrophobic surface [27-29].

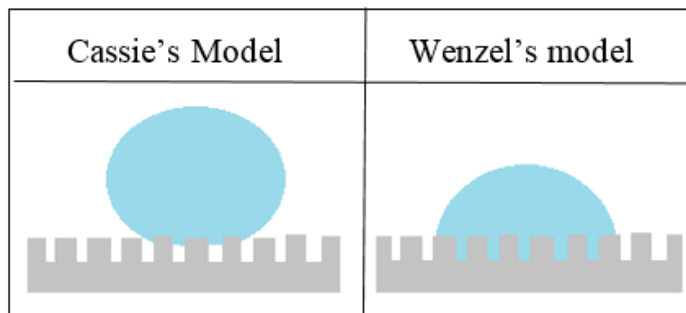


Figure 2.3: Wetting of Rough Hydrophobic Surfaces

In Wenzel's model, there is no air bubbles under the droplet, droplet is in complete contact with surface. So, it completely pins to surface. The Wenzel's model define the experimental contact angle on a rough surface:

$$\cos\theta_W = r \cos\theta_Y \quad (2.3)$$

Where r , θ_w , θ_Y corresponds to the roughness factor defined as the ratio between the real surface area and the ideal surface area, contact angle for rough surface, contact angle for ideal surface, respectively. Equation (2.3) is referred to as Wenzel's model. Compared to smooth surface, rough surface with $CA > 90^\circ$, it will be more hydrophobic when the roughness factor is increased [30]. Additionally, because every surface has some roughness, no surface is completely smooth, so it is known that 'r' is greater than 1. So, by applying r value ($r > 1$) on the equation 2.3, it can be seen that roughness will make hydrophobic surface even more hydrophobic, and hydrophilic surface even more hydrophilic.

In Cassie's model the droplet actually sits on the air bubbles. In this state, droplets will bounce or roll off. This is useful for water repelling and self cleaning surfaces. We can say that Cassie –Baxter state occurs for very very rough surfaces.

$$\cos\theta_w = -1 + \phi_s(\cos\theta_Y + 1) \quad (2.4)$$

where ϕ_s , θ_w , θ_Y percent of solid that is in contact with droplet, contact angle for rough surface, contact angle for ideal surface, respectively. If ϕ_s value of droplet is nearly zero, it means that droplet is sitting mostly on air pockets, so θ_w equals to 180° , and it shows water repelling feature.

3. NATURAL MINERALS

3.1. Diatomaceous Earth

Diatomaceous earth include the siliceous ruins of countless diatoms which is microscopic unicellular aquatic plants. Diatoms are very abundant in which water and light have coincided for an adequate time. When diatoms die, their silica shells amass on the seabed and thick layers of diatom shells are fossilized into diatomaceous earth, or diatomite. Each of the eight thousand and more has a symmetry of skeleton that varies from that of each different species. The skeletons are of the type of crescents, discs, rectangles, triangles, or different geometric figures. Though so small approximately fifty million of them may be available in a cubic inch, the particles have shapes as well as surface adornments that are trademark for the different species. There are elevations, depressions, pores, canals, wave marks, radial lines, which give the divided surface of the DE that gives the surface geology helpful for the accomplishment of superhydrophobic properties of the present development.

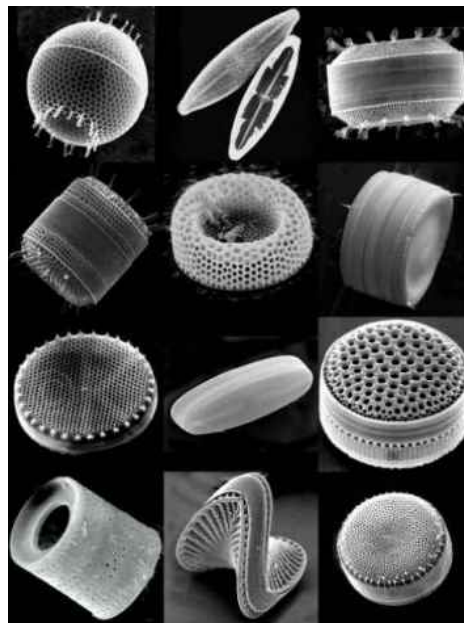


Figure 3.1: Skeleton Symmetries of Diatoms [URL-2]

When the surface is treated in a manner that keep the surface topography but renders the surface hydrophobic. Because it is cheap and has natural porosity and appealing characteristics it is an attractive material for various applications. It can be used as a filter material, filling material, insulation material (heat, sound, electricity), absorbent material, catalyst carrier lightweight building material, refractory manufacturing, as it is silica source it can be used in the production of many chemicals. Diatomaceous earth is soft, friable, fine grained and has low density, low thermal conductivity chemically inert in most liquid and gases. Diatomaceous earth has chemical composition of about 86% silica, 5% sodium, 3% magnesium and 2% iron [31-33].

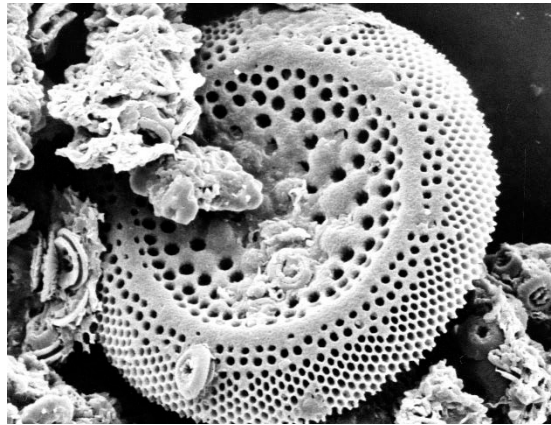


Figure 3.1: SEM Micrograph of Diatomit[URL-3]

To date, DE, has become a model of many research works associated with biomimetic and nanoscale self-assembly [34-36]. Özen et al. used modified diatomite surface by using basic methods using a fluorocarbon chemical that is trimethoxy (3,3,3-trifluoropropyl) silane in addition to the sol-gel fluoro silanization process. As a result of work done, contact angle is 113° [37]. Oliveira et al. put forward a method to make superhydrophobic surfaces using siliceous diatom's skeleton. They use surface chemical modification through fluorosilanization with 1H, 1H, 2H, 2H perfluorodecyltriethoxysilane. As a result of this work, they get contact angle which is 150° [12]. The prominent example was introduced by Simpson and D'Urso with the concept of superhydrophobic powder via surface coated DE [6]. They utilized silanization method by used tridecafluoro-1,1,2,2-tetrahydrooctyl trichlorosilane in their study and as a result of work done, contact angle is 170° . However, although extensive studies have been carried out on the use of DE powder to make

superhydrophobic particles, no single study exists which adequately refers to required possible conditions that can be applicable to any natural powders to make superhydrophobic surface.

3.2. Talc

Talc is a hydrous magnesium silicate mineral. It is the softest mineral and talc has a chemical formula $Mg_3Si_4O_{10}(OH)_2$. Talc is comprised of magnesium hydroxide layer ($MgO \cdot H_2O$) which is between two silicate (SiO_2) layers, there is a three-layer structure as shown in Figure 3.3. Layers are connected by weak van der waals forces that gives talc a platy structure. Talc's SEM micrograph is shown in Figure 3.4. It is hydrophobic, organophilic, chemically inert, platy, and has high thermal and low electrical conductivity [38]. Due to talc's various chemical and physical properties talc can be used in widely areas, for example ceramics, in paint production, roofing, production of insecticidal, rubber and paper industry, cosmetics, pharmacology, animal feed and in fertilizer production.

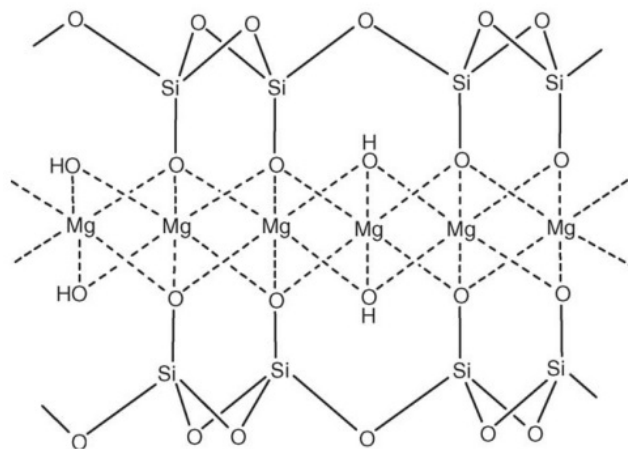


Figure 3.2: Talc Structure

High contact angle on a polished talc surface is measured by Fowkes and Harkins [39]. By using the sessile drop [40] or the wicking technique [41-43] same evaluations have been done again. For all, approximately 80° contact angle were observed. In order to clarify this natural hydrophobic properties of talc mineral, structural reasons have been asserted [40-43]. Because it is siloxane like the basal faces of talc are hydrophobic however the edges of talc are hydrophilic. Rotenberg et al. studied with talc which is untreated. In this work talc's contact angle is 96° [44].

However, Wallqvist et al. also studied with talc which is untreated and the result of this study is 75.2° – 85.7° [45]. Studies shows that, under different conditions talc can be hydrophobic or hydrophilic.

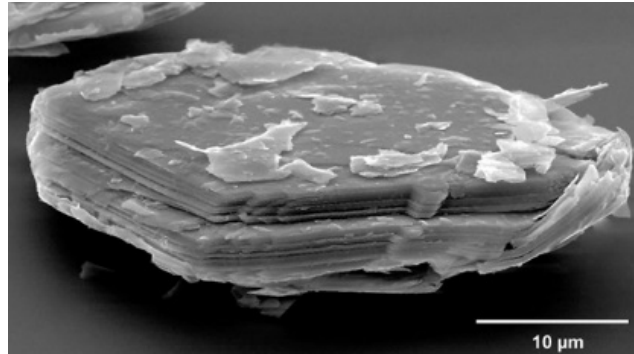


Figure 3.3: Electron Microscope Image of Talc Particle [URL-4]

4. SILANE MODIFICATION

The replicating nature to obtain precise control of parameters gives rise to produce artificial SH surface [3, 46, 47]. The lotus leaf would be the best example of SH texture to be inspired from the nature owing to hierarchical surface topography with waxy content [6, 12, 46, 47]. One of the developed strategies encouraged by nature involves the functionalization of the particle surface via substitution of reactive groups, for example silanols, with mono- or multifunctional silanes [5, 15, 48-51].

Chemical modification is a adaptable method to modify surface wettability. It is possible to present any chemical group on a surface and thus modify its wetting character by using self assembled monolayers (SAM's). Chemical modification using silanes have become ubiquitous in surface science since 1980 [52]. Their popularity in the field of nanotechnology arises due to their high reactivity with hydroxylated surfaces such as silica or alumina.

Specifically, fluoroalkyl-modification of a surface has indicated as a reliable approach both for adequate surface coverage of desired functional groups and fulfilling required conditions of low-surface energy as well as protecting high specific surface area of target particles such as silica [5, 53]. Surfaces fabricated through these materials have some practical applications covering chromatographic process, biomedical devices, corrosion-resistant surface, self-cleaning, anti-icing and so-forth [15, 46, 54-56]. Nevertheless, some new methodologies involving nonwetting by water and many other liquids have also been subject of various researches [29, 57-59].

4.1. Formation of Silane Monolayers

Silanes has high reactivity with hydroxyls covering the surface of oxides. The general reaction of diverse sorts of silanes with hydroxilated surfaces is given in Figure 4.1. High reactivity of silanes can be disadvantage when trying to control the reaction. The reaction rate depend on several factors suchas temperature, solvent,

type of silane, silane structure etc. can be very sensitive to these conditions [60]. Water concentration on the surface and in solution was identified as one of the key factors in the formation of the silane layer.

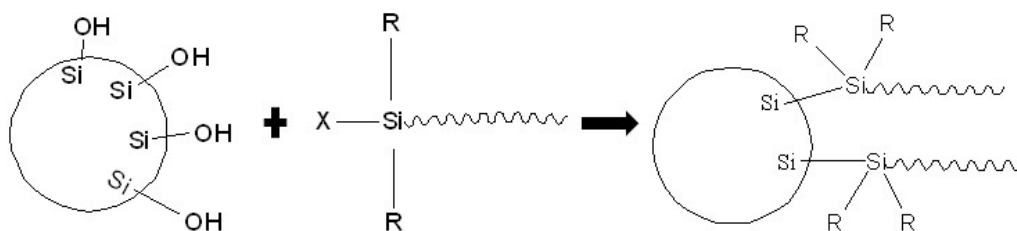


Figure 4.1: Reaction of Silanes with Hydroxylated Surfaces

Rye et al attempted to clarify the role of water in the formation of the reaction of chlorosilanes. It was recognized that the reaction in the absence of water will not proceed to completion since there was not possibility of lateral polymerization [61]. The effect of solvent is closely related to the water content. McGovern et al. compared different solvents and found that the longer the aliphatic hydrocarbon the better the coverage obtained [62]. They also analyzed the capacity of the solvent for the extraction of water from the surface to the bulk. In this case benzene and cyclohexane produce much better coverage than hexane. This also demonstrated that the hydrolysis of the silane takes place in solution and not close to the surface. The type of silane is essential component to take into account since their reactivity varies depending on their chemical nature. In general a silane molecule is composed of a head group ($-\text{SiX}_3$ where X is usually $-\text{Cl}$, $-\text{OMe}$ or $-\text{OEt}$), an alkyl chain of $-\text{CH}_2-$ and the terminal group [63]. In the case of the head group it is known that chlorosilanes are more reactive than alkoxy silanes and form denser layers. However their reactivity makes them very sensitive to the amount of water, which can lead to problems with reproducibility. The number of reactive substituents at the Si can affect also the monolayer formation. For example, Moon et. al have showed that in the case of aminopropyl silanes in toluene, the trimethoxy silane produces multilayers, while dimethylmethoxy silane can not generate complete coverage; methyldimethoxysilane, on the other hand, does not produce multilayers and its monolayer coverage is denser than for dimethylmethoxy silane [64, 65]. The alkyl chain length of the silane also affects packing of the silane layer. It has been shown

through ellipsometry measurements that short alkyl chains tend to form disordered multilayers while longer alkyl chains form ordered monolayers.

Bierbaum et al compared alkylchains of 3, 18 and 30 carbons long and found that the optimal length for a well formed monolayer was [66]. Similarly, Wasserman et al. found that short length alkyl chains do not pack very well and have smaller CA than those of longer silanes and for the chains longer than 7 carbons the CA become independent of the silane used [67].

5. MATERIALS AND METHOD

5.1. Materials

DE mineral (148.62 m²/g surface area) was provided from Beg-Tug Mineral (Ankara/Turkey). Talc mineral (Omyatalc® 5 EXTRA-KS, 23.62 m²/g surface area) was supplied by Omya Mining Co. Inc. (Istanbul, Turkey). Silane reagents, demonstrated in Figure 1, 11-(chlorodimethylsilylmethyl)tricosane (Methyltricosane monochlorosilane or Mtcos-MCS); 1,2-Bis(trichlorosilyl)decane (Deca-BisTCS); Ethyldimethylchlorosilane (Ethyl-MCS); n-butyl dimethylchlorosilane (nBut-MCS); dodecyldimethylchlorosilane (Dodec-MCS); Nonafluorohexyldimethylchlorosilane (FHex-MCS); Dimethylchlorosilaneperfluorooctyl (PFOct-MCS) and perfluorodecyl 1-1H, 1H, 2H, 2H-dimethylchlorosilane (PFDec-MCS) were purchased from Gelest Inc. Reagent grade chloroform, hexane and dichloromethane were purchased from Sigma-Aldrich.

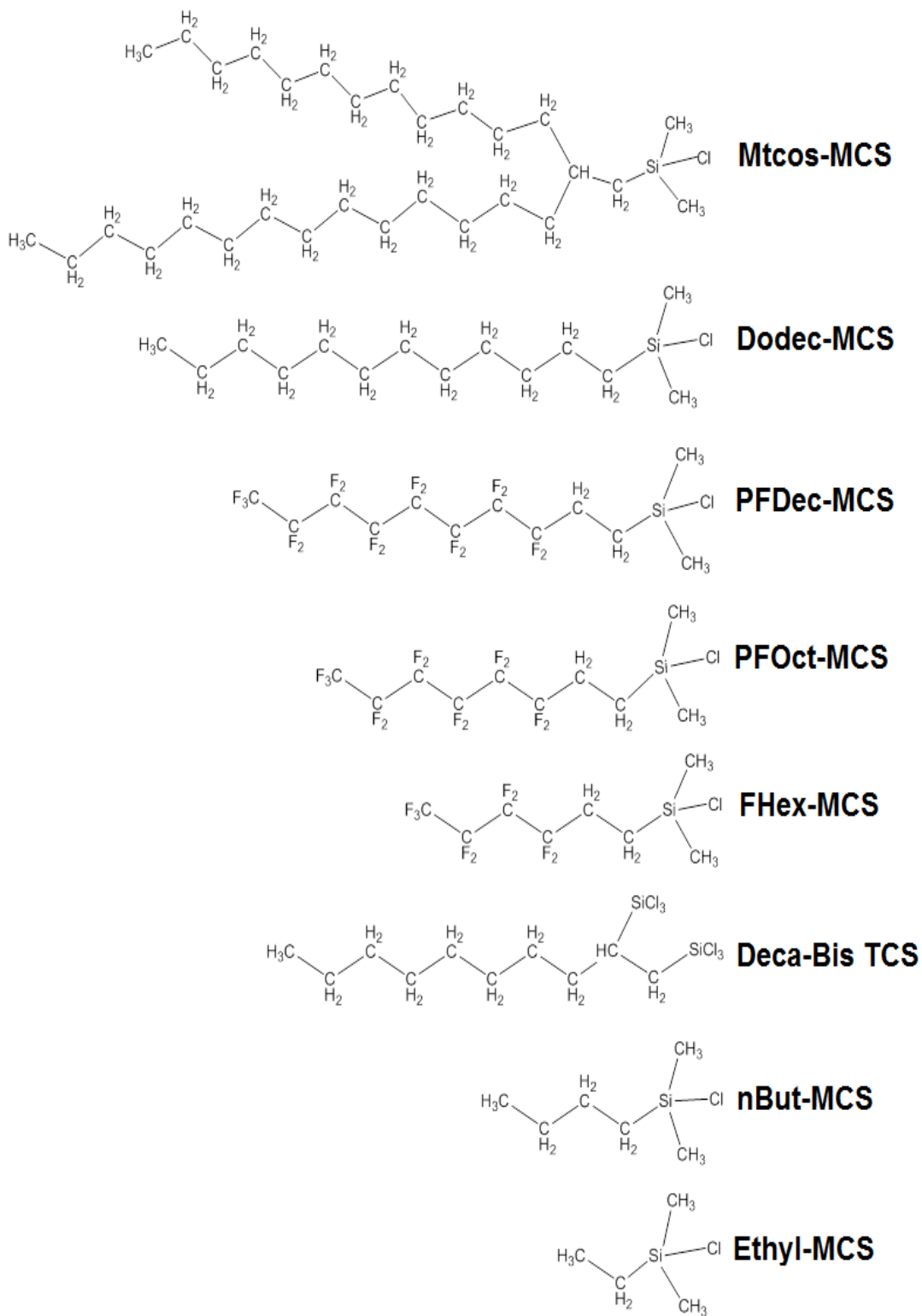


Figure 5.1: Silane Modifiers Used

5.2. Synthesis of Superhydrophobic Diatomaceous Earth

Step 1 (Without pre-treatment). Two grams of DE “as received” were suspended in 60 ml chloroform in 250 ml round-bottom flask. 0.430 ml of PFDec-MCS was dispersed in 20ml chloroform, assuming to graft $5 \mu\text{mol}/\text{m}^2$, and dropwise added to round-bottom flask while the solution was allowed to stir and reflux for 3 h. After DE particles were recovered by filtering at room temperature under vacuum, they were purified by extracting three times in equal volume of hexane and dichloromethane, respectively, to ensure the elimination of any noncovalently bound chlorosilane derivatives and other surface contaminants. After extraction process, the DE particles were collected, transferred to vials, and dried at room temperature for 1 day.

Step 2 (Calcination used). In this step effect of calcination on wetting properties of natural mineral powders was studied. Different from the first step, two grams of two DE samples, calcined at $400 \text{ }^\circ\text{C}$, were suspended in 60 ml chloroform in different reaction flasks. 0.430 ml and 0.860 ml of PFDec-MCS were dispersed in 20 ml chloroform and then dropwise added to DE suspension under reflux with stirring, assuming to obtain $5 \mu\text{mol}/\text{m}^2$ and $10 \mu\text{mol}/\text{m}^2$ surface coverage, respectively. The reaction procedure was continued as described in step 1.

Step 3 (Different Grafting Densities used). In this step effect of different grafting densities on wetting properties of calcined mineral powders was studied. The third step for the functionalization of DE surface was analogous to the second step with only differences of surface grafting densities. In this case, 0.213 ml and 0.640 ml of PFDec-MCS were used to attain $2.5 \mu\text{mol}/\text{m}^2$ and $7.5 \mu\text{mol}/\text{m}^2$ surface coverage. The reaction procedure was identical to step 1.

Step 4 (Various silanes used). In this step, several silane derivatives, which are in turn 0.520 ml of Mtcos-MCS, 0.580 ml of Deca-BisTCS, 0.304 ml of nBut-MCS, 0.536 ml of Dodec-MCS, 0.568 ml of FHex-MCS, were used to reach $7.5 \mu\text{mol}/\text{m}^2$ surface coverage for the DE specimens calcined at $400 \text{ }^\circ\text{C}$. The reaction procedures were then continued as described in step 1.

Step 5 (Different mineral used). The optimal results of each step was selected to apply on talc mineral powder. Two grams of two talc samples, calcined at $400 \text{ }^\circ\text{C}$, were used instead of DE. 0.085 ml and 0.113 ml of PFDec-MCS was preferred to

achieve the surface coverage of 7.5 $\mu\text{mol}/\text{m}^2$ and 10 $\mu\text{mol}/\text{m}^2$, respectively. All following steps were analogous to step 1.

All the silane treatment steps employed, abbreviations of samples and grafting densities are summarized in Table 2.

Table 2: Summary of Surface Functionalized Minerals

Sample	Mineral	Calcination ($^{\circ}\text{C}$)	Silane	Grafting Density ($\mu\text{mol}/\text{m}^2$)	Step
HME-Bare	DE	None	none	None	-
HME-Blank	DE	400	none	None	-
HME-1	DE	None	PFDec-MCS	5	1
HME-2	DE	400	PFDec-MCS	5	2
HME-3	DE	400	PFDec-MCS	10	2
HME-4	DE	400	PFDec-MCS	7.5	3
HME-5	DE	400	PFDec-MCS	2.5	3
HME-6	DE	400	PFOct-MCS	7.5	4
HME-7	DE	400	FHex-MCS	7.5	4
HME-8	DE	400	nBut-MCS	7.5	4
HME-9	DE	400	Ethyl-MCS	7.5	4
HME-10	DE	400	Dodec-MCS	7.5	4
HME-11	DE	400	Mtcos-MCS	7.5	4
HME-12	DE	400	Deca-BisTCS	7.5	4
HME-13	Talc	400	PFDec-MCS	7.5	5
HME-14	Talc	400	PFDec-MCS	10	5

5.3. Characterization Methods

5.3.1. Particle size and surface area (Brunauer-Emmett-Teller) analysis

Particle size distribution of minerals was determined via Malvern-Mastersizer Hydro2000S in aqueous phase. The Brunauer-Emmett-Teller (BET) surface area of particles was determined by nitrogen adsorption by using Quantachrome NOVA

2000e adsorption instrument after degassing of samples at 150°C for 6 h. In this study, BET analysis was performed in order to see the effect of calcination on the mineral surface area and also recognize the effect of grafting density on sample surface.

5.3.2. FESEM (Field Emission Scanning Electron Microscopy) analysis

The surface morphology and microstructure of both “as received” and calcined DE minerals were studied by using Zeiss EVO 40 Field Emission Scanning Electron Microscopy (FESEM). The materials were introduced onto a conductive carbon tape and coated with gold to prevent charging.

5.3.3. XRF (X-ray fluorescence Spectrometer) analysis

The chemical content analysis of “as received” and calcined DE and Talc were performed by Thermo Scientific ARL Advant’x X-ray fluorescence Spectrometer. In the present study, XRF analysis was performed to understand that how the calcination effects the content of mineral particles.

5.3.4. XPS (X-ray Photoelectron Spectrometer) analysis

Chemical composition of the surface of samples was analyzed with K-Alpha™+ X-ray Photoelectron Spectrometer (XPS) System. In the present study, XPS analysis was provide us to observe that calcination changes the chemical composition of mineral particles.

5.3.5. TGA (Thermogravimetric analysis)

Thermogravimetric analysis of samples was examined with PerkinElmer STA8000. Samples were heated to 1000°C at 10°C/min under the controlled atmosphere (N₂ gas). The percent weight lost up to 1000°C was used to evaluate thermal stability of grafted layers and to predict the grafting density of customized DE.

5.3.6. Contact Angle analysis

Attension Theta Lite Optical Tensiometer was used for static and dynamic contact angle measurements. The static measurements were performed by dispensing a water droplet with an average volume of 4 µL whilst dynamic contact angle measurements were employed with different grafting densities of DE.

5.3.7. Water Vapor Affinity Measurements

In order to examine the affinities of HME-blank, HME-2 and HME-3 to water, following steps have been taken: All materials were suspended in chloroform and ultrasonicated for 1h in order for X materials to be dispersed thoroughly in solvent. Then, the solutions were kept at room temperature for 24h. By using a shadow mask, gold electrodes with 100nm thickness, 17 μm gap and width of 1500 μm were evaporated thermally on the glass substrates. In order to form thin films of each material, 2 μL of each solution was drop casted between the gold electrodes. After preparation of thin films of each material, the experimental setup consisting of 2-channel gas flow system with required software and equipment was used. Massflowmeters (MFCs) control the system at flows ranging between 0 and 1000 sccm and send the flow of pure inert nitrogen (dry N_2) into water bubbler to produce wet nitrogen (wet N_2). A commercial humidity sensor (Sensirion, Switzerland) and a sourcemeter (Keithley, model 2636A, USA) were synchronously used to record the real-time humidity and electrical response, respectively. Water affinities of HME-blank, HME-2 and HME-3 were investigated by exposing prepared samples to 86% RH at room temperature and measuring the change in the electrical response due to water adsorption.

6. RESULT AND DISCUSSION

Since the present study designed to develop a model work for the natural powder with low surface energy and to achieve desired degree of superhydrophobicity in controlled manner, optimized modification conditions that were anticipated to expand surface cover age of powder were pursued on DE. The obtained conditions were taken as model work and applied to Talc mineral, which was preferentially chosen due to the fact that it has peculiar affinity toward water. The methodology based on the chemical content, morphological character and physical properties of chosen powders are the key aspects to maximize grafting density. In this respect, following results highlight several fundamental features of the inherent textures mentioned above.

6.1. XRF, XRD, BET, ParticleSize and SEM Analysis of As-received and Calcined DE Minerals

The chemical composition, surface area and particle size data of the “as-received” DE are given in Table 3. The content of siliconoxide is 65.5% for crude DE which is less than typical silica content of reported crude DE [6]. As-received samples contain chemical bonded water in their crystal structures.

Table 3: Chemical Composition Analysis of “As-received” Sample (wt.%)

Mineral	SiO ₂	MgO	CaO	Fe ₂ O ₃	Al ₂ O ₃	TiO ₂	K ₂ O	SO ₃	Loss on ignition
Diatomite	65.5	1.75	2.39	2.61	7.89	0.28	1.45	0.13	17.6

X-ray diffraction phase analysis of the as-received DE is illustrated in Figure 6.1. The broad hump in the vicinity of the crystalline peaks (from 10° to 40°) is typical for DE that indicates an amorphous phase as well as crystalline phases. According to the semi-quantitative analysis, the main structure of DE consists of cristobalite (β -

SiO₂), quartz (SiO₂), hypothetical silica (SiO₂), opaline silica (SiO₂•nH₂O), sanidine (KAlSi₃O₈), calcite (CaCO₃), muscovite (KAl₂(AlSi₃O₁₀)(F,OH)₂) and dolomite ((Mg,Ca)(CO₃)₂). XRD phase analysis of the calcined DE is given in Figure 6.2. The broad hump in the vicinity of the crystalline peaks (from 10° to 40°) is typical for DE that shows an amorphous phase as well as crystalline phases. According to the XRD analysis, the main structure of DE calcined at 400°C consists of hypothetical silica (SiO₂), cristobalite (β-SiO₂), quartz (SiO₂), sanidine (KAlSi₃O₈), calcite (CaCO₃) and dehydroxlated muscovite. Also, opaline silica (SiO₂•nH₂O) is decomposed and the cristobalite peak increase. In the DE calcined at 800°C, calcite peaks disappeared as well as quartz peak increased. The XRD result of DE calcined at 1000°C indicated that the silica structures transformed to cristobalite crystalline phase. Also, anorthoclase (KAlSi₃O₈) and diopside ((Ca,Mg)(Si₂O₆)) crystalline phases occurred in higher temperatures.

The step 1 was employed to over simplify substitution of silanols with fluorocarbon substituents. In previous studies, [6, 12] preference of crude (uncalcined) DE has been reported for the synthesis superhydrophobic powders. By contrast, samples recovered from the first step (HME-1) have not fulfilled the required conditions for hydrophobicity. Note, however, that in order to be suitable for the silylation of any surface of silica based particle, it is essential for the SAM precursor to contact and bound to particle surface without confronting any obstacle [6, 68]. It can be deduced that chemical contaminants like organic impurities and uptaken water have more profound effects for the samples with low percent silica content compare to that of reported counterparts.

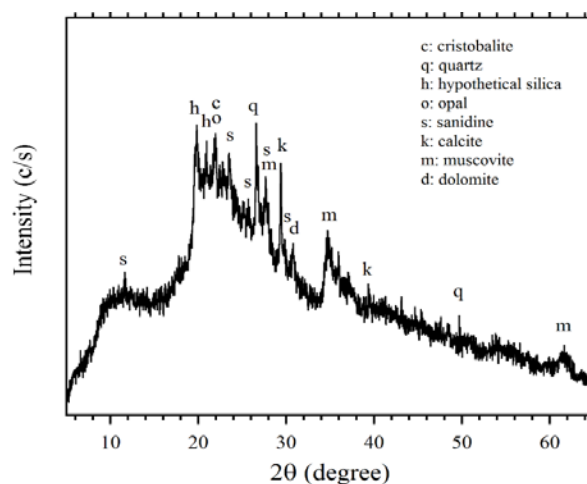


Figure 6.1: The XRD Patterns of the As-received DE

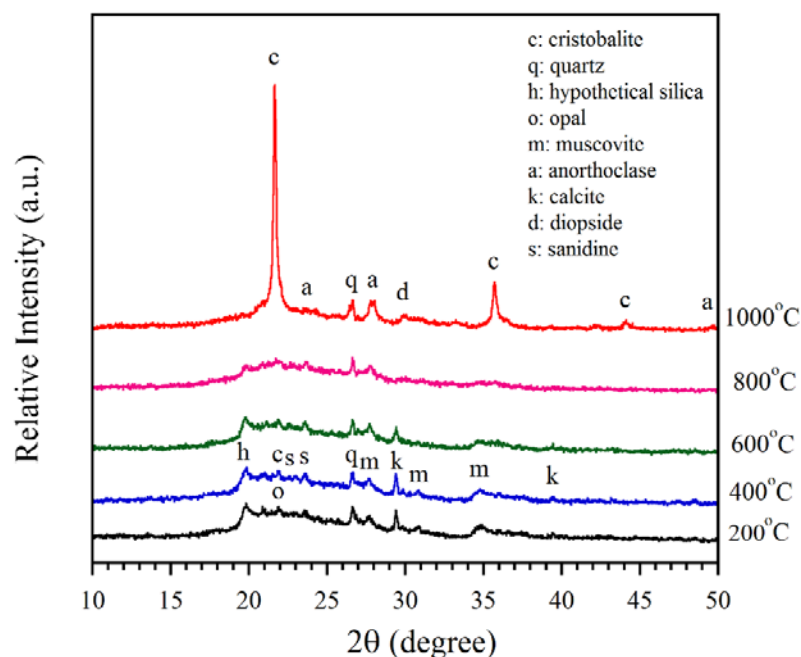


Figure 6.2:The XRD Patterns of the Calcined DE

The thermogravimetric analysis (TGA) of as-received raw materials is given in Figure 6.3. In the TGA curve of diatomite was observed a total weight loss of about 16% for 1000°C. In the first weight loss, the dehydration of the diatomite takes place between 20 and 200°C which corresponds to the loss of free water physically absorbed on the surfaces and in the pores of diatomite particles. The mass losses in the range of 200-500°C can be attributed to the removal of organic impurities, around 600°C probably to removal of chemically absorbed water molecules of amorphous opaline silica ($\text{SiO}_2 \cdot n\text{H}_2\text{O}$). The use of gradual calcination studies were performed, in which the change in percent silica content, particle size and surface area were screened according to various calcination temperatures for an attempt to optimize reaction conditions given in Table 4. In agreement with previous reports, [6] calcination can be performed to eliminate organic contaminants and physically adsorbed water that can occupy the active features of the DE and interfere with bonding the SAM precursor to the DE surface. Table 4 shows the XRF, BET and particle size results of DE minerals calcined at different temperatures.

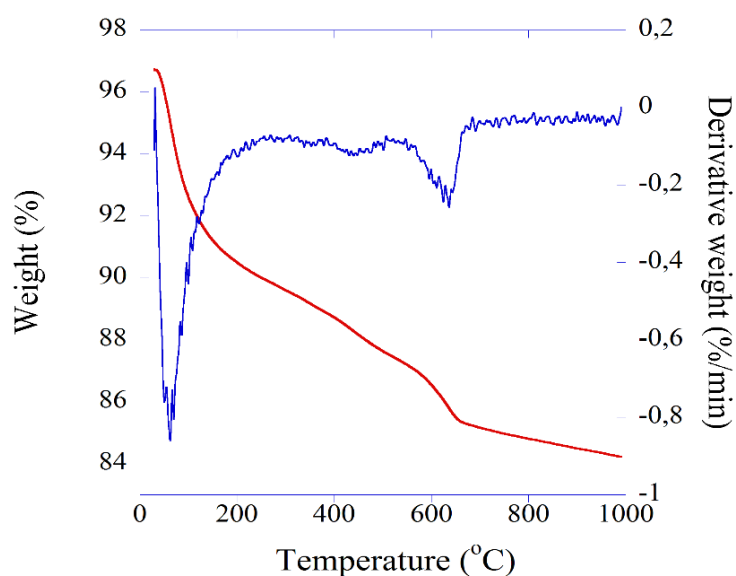


Figure 6.3: TGA Curves of As-received Diatomite

As seen in Table 4, the amount of silica (SiO_2) and other oxide compounds increased within crease of calcination temperatures whilst the surface area decreases. It's known that, customization of the surface to load hydrophobicity entails keeping high specific surface area and excess amount of active features such as silica with eliminated contaminates and physisorbed water. In the light of this information and recent studies, [15, 48, 49] DE calcined at 400°C was considered to be the best one that fulfills the desired conditions. SEM micrographs of DE particles given in Figure 6.4.

Table 4: Effect of Calcination of DE on Chemical Composition , Surface Area and Partical Size Analysis (wt.%)

Calcination temperature	Chemical Analysis wt%		Surface area , m^2/g	Mean particle size, μm
	SiO_2	Other oxides		
DE("As-received")	65.50	16.50	148.62	6.93
200°C	68.30	19.61	117.75	7.14
400 °C	71.00	18.86	116.98	7.00
600 °C	72.20	19.74	106.98	6.76
800 °C	76.00	20.85	88.65	7.43
1000 °C	78.27	21.73	1.02	8.13

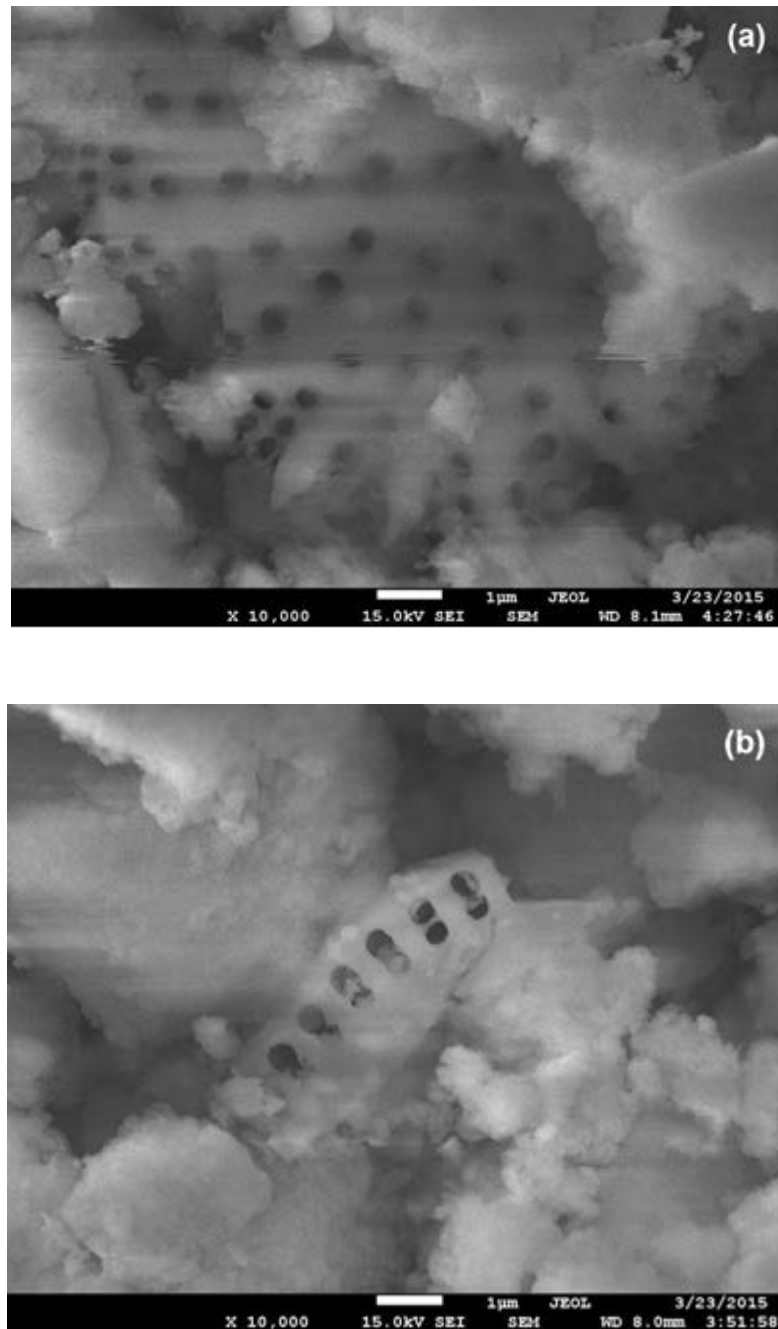


Figure 6.4: SEM micrographs of a) “As-received” DE, b) Calcined DE at 400 °C

6.2. Water Vapor Affinity Results

In step 2, For the practice of efficacy of calcination on the surface modification of DE particles, grafting procedure (PFDec-MCS) described. Here in, the effect of grafting density on the water vapor affinity of the diatomaceous has also been investigated. As specified before, the object is to see what happens when DE is functionalized with silane moieties with increasing grafting density interms of water affinity. Hence, thin films of these DE based specimens were readily developed on

the surface of gold electrodes separated with 3 μ m gap to compare electrical properties of the min the presence of water molecules. As seen in Figure 6.4, depicting adsorption and desorption characteristics of each material, the red, blue and green dashed lines represent the variations in the resistance of HME-blank, HME-2 and HME-3, respectively. The electrodes coated with these materials measured changes in the resistance due to adsorption and desorption of water vapour. The real-time relative humidity (RH) values in the test cell were simultaneously collected with a commercial Sensirion sensor during measurements. This sensor displayed 15% RH when the test cell was purged with dry N₂ while it became 86% RH when only wet N₂, obtained by sending dry N₂ through water bubbler kept at a constant room temperature. We have sent dry and wet N₂ consecutively in 200s periods in order to investigate the affinity of each electrode to water during adsorption process. When fully dry nitrogen has been sent to the test cell, maximum resistances (R_0) of HME-blank, HME-2 and HME-3 have been obtained as $2.47 \times 10^8 \Omega$, $2.40 \times 10^8 \Omega$ and $2.38 \times 10^8 \Omega$, respectively. The water affinity of each material has been defined as ($\Delta R/R_0$), where R_0 is initial (maximum) resistance of the film and ΔR is the change in the resistance of the film [69]. The maximum responses of HME-blank, HME-2 and HME-3 have been found as 102.4%, 99.7% and 95.9%, respectively. As a consequence of increase in the RH giving rise to increase in the amount of adsorbed or capillary-condensed water molecules, the resistances of thin films of each material have decreased according to the experimental results. It has also been seen that HME-blank has performed highest affinity towards water molecules while this affinity has decreased as grafting density increased, leading us to considering that varying grafting density could be the key parameter to tune the hydrophobic characteristic of relevant diatomaceous.

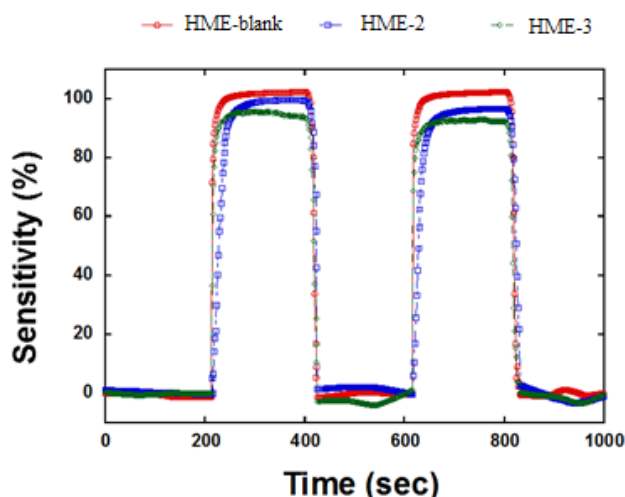


Figure 6.5: Effect of Grafting Density on Water Vapor Affinity of Samples

6.3. TGA, BET, XPS and Contact Angle Analysis of Modified DE Samples

In step3, DE powders were subjected to grafting procedure defined in step to assess whether and how tunable hydrophobic surface are produced. The reliability of measures was increased by rendering the grafting densities that are the grades between the values indicated in step 2.

Table 5: Influence of Reaction Parameters on Key Features of Treated DE Samples

Sample	Grafting Density ($\mu\text{mol}/\text{m}^2$)	% Weight Loss	BET“C Constant	BETArea (m^2/g)	Contact angle
HME-Blank	None	8.20	146	117	35.5 ^o
HME-5	2.5	14.64	35	119	157 ^o
HME-2	5.0	17.29	25	86	163 ^o
HME-4	7.5	18.45	24	109	165.5 ^o
HME-3	10.0	18.92	21	83	166.5 ^o

In an attempt to optimize analysis parameters and to evaluate correlation between them, comparative screening study was carried out. The data of the samples gathered from step 2 and step 3 were synergistically examined as well as their results from TGA weight lost, BET surface area, and contact angle measurements were depicted in Table 5. It is significant to note that in addition to surface coverage estimation from TGA analysis, a strong correlation between BET “C constant” and surface

energy has previously been reported in the literature [5, 70-73]. The required features of hydrophobic materials are a low content of hydrophilic group due to high grafting density (as represented by TGA weight loss), and a low surface energy (a low BET “C constant”) giving rise to high contact angle. Therefore, it is concluded for the samples that the higher the amount of fluoroalkyl grafting density on the particle surface is, the higher the amount of percent weight loss in TGA, the lower the surface energy (the lower BET “C constant”) leading to gradual increase in static contact angle. Keeping of a considerably high specific surface area is another desired condition for surfaces to be liquid repellent, as it demonstrates protection of multiscale surface roughness that is favorable for creating a solid-liquid-air interface. Nevertheless, the degree to which the surface area is altered during the concerted silane substitution is uncertain however, it is anticipated to be as great as or lower than the “blank” sample [5].

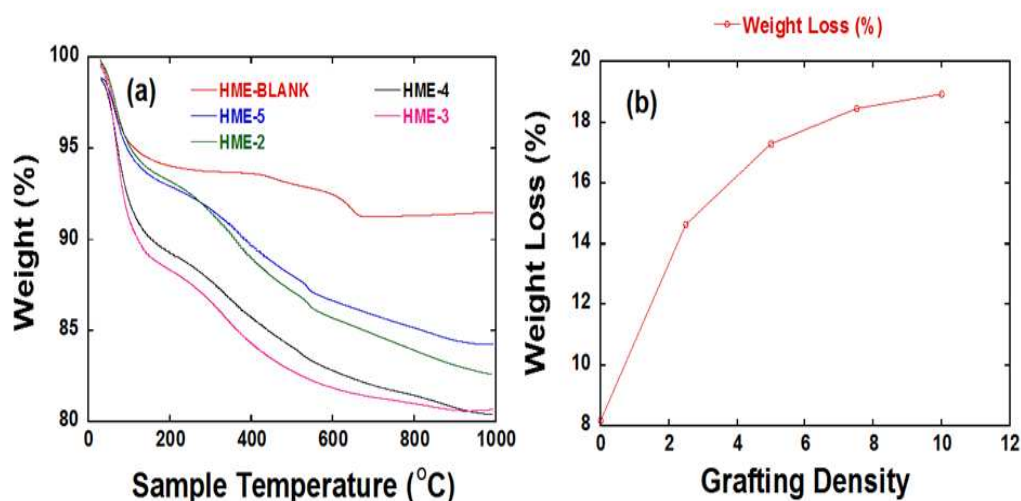


Figure 6.6: TGA Thermograms of PFOct-MCS grafted samples, b) Effect of PFOct-MCS grafting Density on TGA Weight Loss

According to Table 5, Figure 6.6a,b HME-Blank under went to modest % 8.20 weight loss due to desorption of strongly bonded species or condensation of silanols, where as percent weight loss gradually increase sup to %18.92 in HME-3 owing to increment of grafting density. This increase was also confirmed by the gradual decrease in BET “C constant” that proves decreasing of surface energy with respect to successful increasing of grafting density. Moreover, it is apparent from Figure 6.6b that there is a decrease in the increment of percent weight loss differences

between the samples from HME-blank to HME-3. We suppose that surface of DE particles started to saturate with an increase in grafting density and steric hindrance become more prominent due to the saturation. Specifically, as light difference in percent weight loss between HME-4 and HME-3 is the most meaningful indicator of saturation.

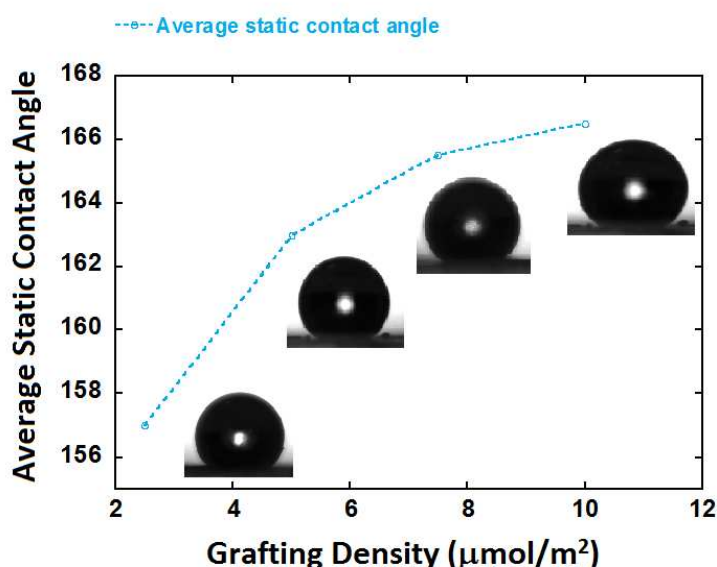


Figure 6.7: Effect of Grafting Density on Average Static Contact Angle

Further, this phenomenon is proved by the contact angle measurements that follow the same trend. The decrease in the rise of contact angle differences between the samples from HME-blank to HME-3 is attributed to diminish in the amount of free silanols on the surface of the particles, which bring about increasing of wettability. Additional evaluation of surface modification given in Figure 6.7. Other eligibility criteria of superhydrophobicity of particles are defined as having both contact angle hysteresis (CAH) and sliding angle (SA) < 10 [19, 20, 74]. Dynamic contact angle analysis was carried out with water droplets by using both sliding (measurement on a slope) and extension-contraction methods (0.2 $\mu\text{L}/\text{s}$ step increase and decrease) for different materials. As expected, “as-received” DE and HME-Blank samples are completely wet. Nevertheless, HME-5 and HME-2 displayed conclusive results during dynamic experiments. This is a consequence of low surface energy of DE particles during the addition of a water droplet on functionalized DE surface that caused loosely adhered DE particles coming off the glass substrate and accumulated around/in to the water beads. In some circumstances, water beads reached and wet

the surface of glass substrate. In consistent with literature, this behavior is reasonable in the paint of the study of “liquid marbles” in which droplets of ionic liquid or high surface tension water are efficiently coated by particles having low surface energy such as a sub-micrometer oligomeric tetrafluoroethylene(OTFE) particles or hydrophobized silica [75, 76].

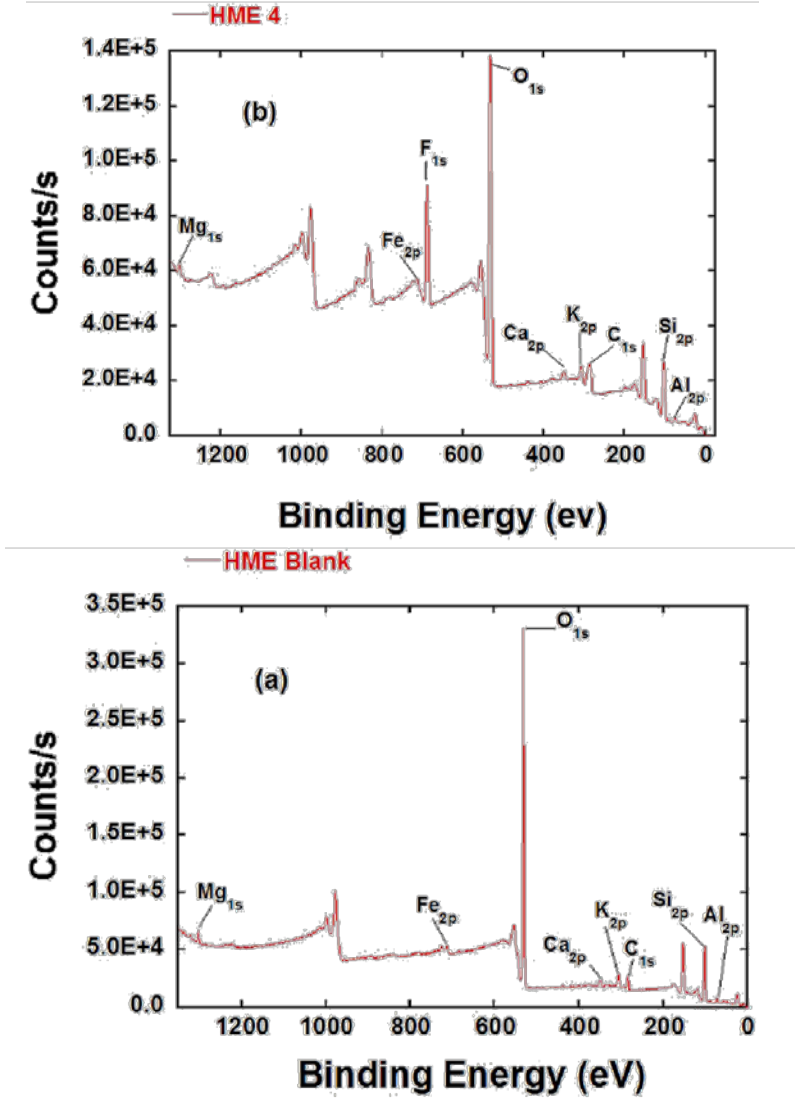


Figure 6.8: XPS Survey Spectrums of a) HME-Blank, b) HME-4

The surface grafting of DE particles are further borne out by X-ray photoelectron spectroscopy. Inasmuch as XPS estimate of the chemical composition of the few upper most layers of the surface and DE has sophisticated architecture, it was used to get further insight into the nature of functional groups on the surface instead of comparing the degree of grafting densities depending on chemical content of samples in Table 5. Thus, HME-Blank and HME-4 were chosen to compare the differences in

surface composition. In present work, Al_{2p}, Si_{2p}, K_{2p}, Ca_{2p}, O_{1s}, Fe_{2p} and Mg_{1s} signals (in Figure 6.8a, b) account for the constituents that the natural DE mineral contains. C_{1s} signal at 286.4eV is owing to alkyl group of silane structure bonded to DE surface (Figure 6.8 b) whereas the expected weak peak of C_{1s} at 284.04eV in HME-Blank (Figure 6.8 a) might be due to the impurities. The sharp F_{1s} peak at 688.4 eV is assigned to C-F bonds at silane tail chains, which confirm the successful grafting of fluorosilanes on DE particles.

6.4. Advancing and Receding Contact Angles Results

However, HME-4 and HME-3 did not display such an unwanted behavior that was a phenomenon on demonstrating strong adhesion between these particles and glass substrate to measure dynamic contact angle. For the former one, sliding technique (with tilted angle of 7°) was carried out to measure the advancing-receding contact angles and the result is given in Figure 6.9a. The surface resulted in $\theta_{adv}/\theta_{rec}=166.52/139.71$ (CAH \approx 26.81). Large water bead stuck to substrate surface even with tilt angle of 90° as seen in Figure 6.9b. The result obtained from sliding method was also confirmed with extension-contraction method, which gave rise to $\theta_{adv}/\theta_{rec}=166.17/139.98$ (CAH \approx 26.19) (see Figure 6.9c and d).

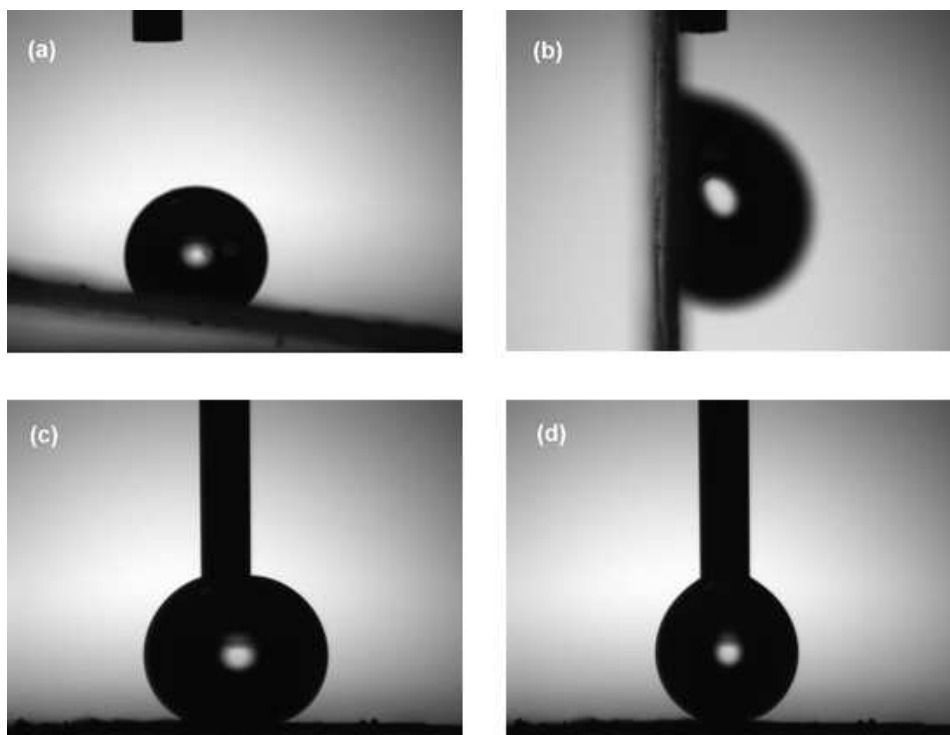


Figure 6.9: Shape of Water Droplets Illustrating Wetting Behavior of HME-4 a) Inclined Surface for Advancing and Receding Contact Angles, b) 10 μl of Water Droplet Pinned to the Surface of HME-4, c) Water Droplet Extended to 5 μl for Advancing Contact Angle, d) Water Droplet Contracted to 4 μl for Receding Contact Angle

High contact angle hysteresis and large water droplet stuck to substrate are the indicators of rough surface with complete wetting between the droplet and interface of the surface. For the latter one, sliding method could not be used due to the fact that water beads rolled off the surface with even quite low tilt angle. Namely, we attempted to measure dynamic contact angle on inclined surface (7° tilt angle) via dispensing $10\mu\text{L}$ droplet, but the droplet spontaneously rolled off the surface. To stabilize the water bead on the surface, both tilt angle and water droplet volume were decreased to 4° and $3.5\mu\text{L}$, respectively. Interestingly, droplet did not dispense on the surface even though dispenser of the tensiometer was triggered several times. As a final trial, the tilt angle and droplet volume were kept constant (4° , $3.5\mu\text{L}$), yet the distance between the surface and dispenser was increased 2-fold. The droplet was seen rolling off the surface. Therefore, extension-contraction method was preferred on a horizontal surface of HME-3 to conduct dynamic contact angle measurement. The surface resulted in $\theta_{\text{adv}}/\theta_{\text{rec}}=166.15/165.38$ ($\text{CAH}\approx 0.77$) (see Figure 6.10a,b). This result is consistent with highly silylated and homogeneous surface with extensive fluoroalkyl content.

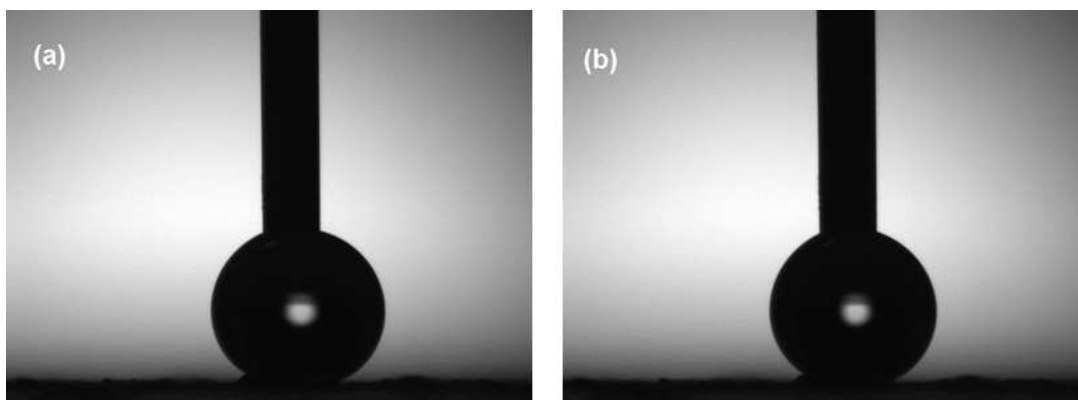


Figure 6.10: Shape of Water Droplets Illustrating Wetting Behavior of HME-3 a) Water Droplet Extended to 5 μl for Advancing Contact Angle, b) Water Droplet Contracted to 4 μl for Receding Contact Angle

6.5. Effects of Different Silane Structures and Degree of Functionality

Additional insight into low surface energy particles has been gained by varying silane structures and degree of functionality. Chloro-functional silanes were preferentially used over the alkoxy-functional silanes for the reason that the literature has emphasized the importance of using chloro silanes for the direct substitution with surface silanols in the absence of water [5, 77]. Albeit excess amount of surface water has regularly been notified to contribute silanol substitution via chloro-alkoxy-functional groups [78-80], surface customization by grafting silanes in anhydrous conditions ought to minimize self-condensation of hydrolyzed silane agents that result in undesired side products [78, 81]. Another additional case reported in the literature is associated with the superiority of monochlorosilanes over multifunctional analogues in terms of producing homogeneous monolayer with the lower silanol content as well as having the better water repellent character for precipitated silica [5]. In as much as the surface of DE is more similar in composition to that of precipitated silica, [6] monochloro silane was utilized in between step 1-3 to investigate the effects of a fore mentioned factors as well as in step 4 to explore the influence of the chain length and several silane structures. The silane modifiers were chosen according to availability in market and desire to maximize the sorts of silane structures.

In Step 4, further exploration for the key features of DE particles with respect to changing silane structures is examined. For the samples grafted with fluoroalkyl silanes (PFDec-MCS, PFOct-MCS and FHex-MCS), the contact angles under go

gradual decrease with decreasing chain length, indicating that the longer the fluoroalkyl chain length is, the higher the hydrophobicity that causes gradual decrease in the surface energy (See Figure 6.11 a-c). In accordance with the present result, the previous work has indicated that increasing fluoroalkyl chain length causes remarkable decrease in BET “C constant”, which also proves the lower surface energy and provides additional explanation for gradual decrease of contact angles [5]. For the elaboration of the effect of silane structures, DE particles were grafted with silane with long alkylchain. Inhere, hydrophobic feature of Dodec-MCS (Figure6.11d) is comparable to water- repellency properties obtained with the most fluorinated silane (PFDec-MCS). This finding is rather favorable from ecotoxic approach because recent studies revealed the persistence and bio accumulation potential of fluorinated alkyl substances, which is the key challenge for bio inspired materials [5, 82-85]. Compared with fluoroalkyl chain, there is considerable decrease in contact angle with decreasing hydrocarbon chain lengt has expected (Figure 6.11e, f).

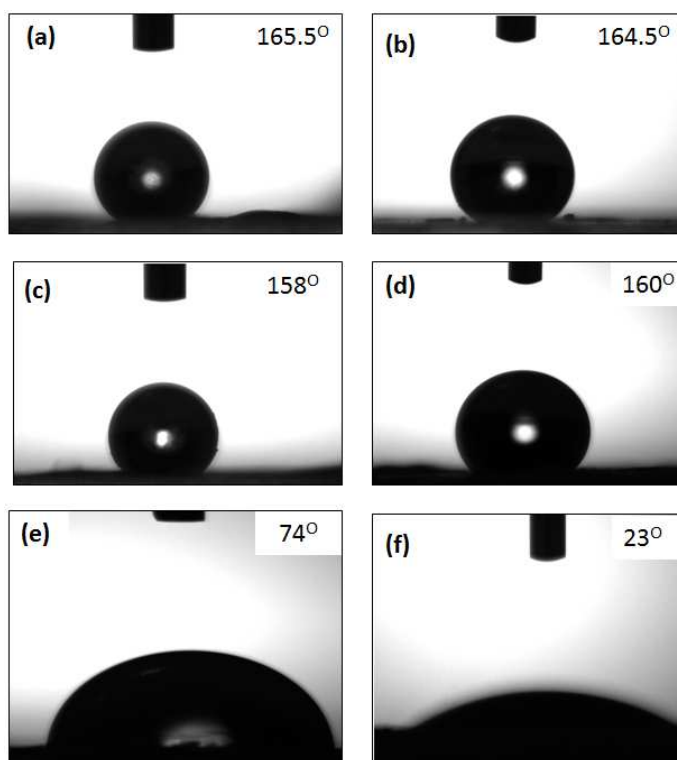


Figure 6.11: Changes in Water Contact Angle with regards to Different Silane Structures a) PFDec- MCS Modified DE (HME-4), b) PFOct-MCS Modified DE (HME-6), c) FHex-MCS Modified DE (HME-7), d) Dodec-MCS Modified DE (HME-10), e) nBut-MCS Modified DE (HME-8), f) Ethyl-MCS Modified DE (HME-9)

Another comparative screening study concerning hydrophobicity was conducted to elucidate the effect of chain variation and degree of functionality of silane substances. Compared to Dodec-MCS, Mtcos-MCS displayed wettable characteristic inspite of carrying branched and long hydrocarbon chain (Figure 6.11a). This result may be explained by the fact that bulky structure of used silane makes steric effect more dominant and inhibits reaction that gives rise to remaining much of the silanols with out substitution and significantly increased heterogeneity. As to Deca-Bis TCS, it displayed higher hydrophilicity with respect to Dodec-MCS (Figure 6.12b). This result is in accord with recent literature [5]. Indicating that multifunctional silane treatment cause remaining of higher silanols content.

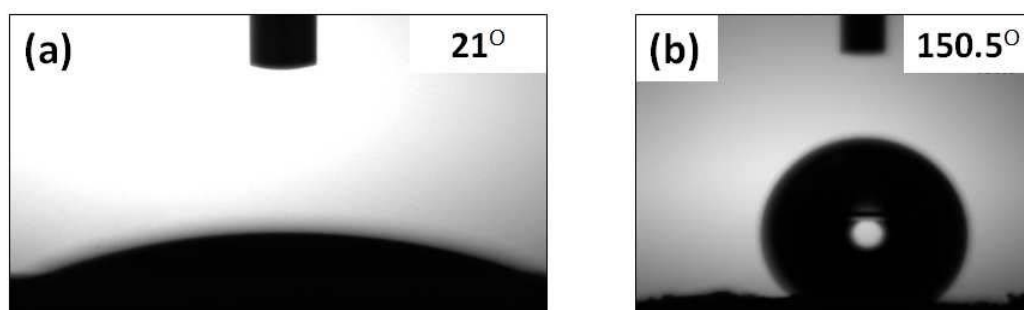


Figure 6.12: a) Effect of Chain Variation on Water Contact Angle (HME-9), b) Effect of Degree of Functionality on Water Contact Angle (HME-12)

6.6.Talc Mineral Results

Taken together, preparation conditions of inherent texture, ideal grafting density and reaction conditions have been optimized and applied to talc as depicted in step 5. The chemical composition and BET analysis of the as-received talc is given in Table 6. The content of silicon oxide is 59.2% for talc. As-received sample of talc contain chemical bonded water in their crystal structure.

Table 6: Chemical Composition and BET Analysis of “As received” Talc (wt.%)

Mineral	SiO ₂	MgO	CaO	Fe ₂ O ₃	Al ₂ O ₃	SO ₃	Loss on ignition	BET(surface area) (m ² /g)
Talc	59.2	30.8	1.82	0.30	0.26	0.01	7.57	23.62

Particle size analysis of the as-received talc is given in Table 7. Particle size distributions show that the size of 90% of talc (d90) are less than 17.6 μm . Mean particle size (d50) of talc is around 5.9 μm . The TGA curve (Figure 6.13) of the talc indicated two main decomposition steps at 500-650 $^{\circ}\text{C}$ and 800-1000 $^{\circ}\text{C}$ respectively. The first decomposition step can be attributed to the dehydroxylation of the layers of chlorite, while the second stage is characterized the loss of structural water due to the dehydroxylation of the mica (OH) layers of talc[86].

Table 7: Particle size analysis of the as-received talc

Mineral	d(0.1)	d(0.5)	d(0.9)
Talc	1.98 μm	5.96 μm	17.66 μm

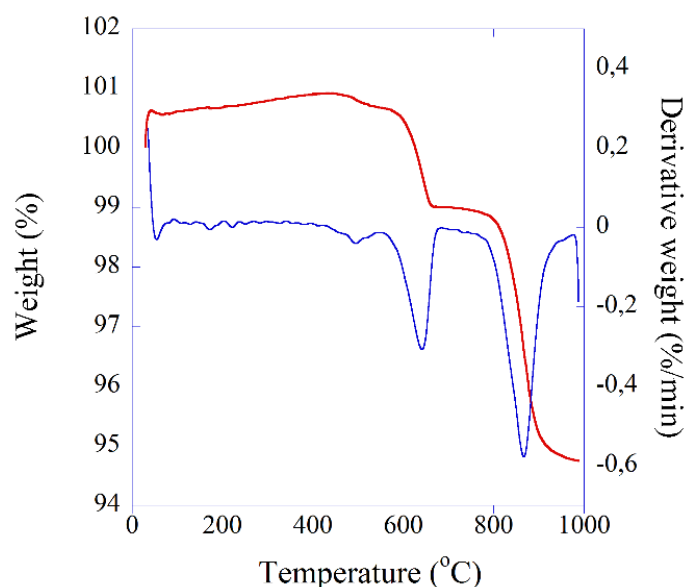


Figure 6.13: TGA Curves of As-received Talc

The SEM image of as-received talc sample are shown in Figure 14. XRD pattern of talc mineral calcined at 400 $^{\circ}\text{C}$ contains magnesium silicate hydroxide ($\text{Mg}_3\text{Si}_4\text{O}_{10}(\text{OH})_2$) crystalline phase (Figure 6.15). Talc mineral, preferred on account of peculiar affinity towards water, performs either hydrophilic or hydrophobic behavior depending on relative humidity [44]. This dichotomy has been overcome through grafting the talc surface that has given rise to permanent water repellency.

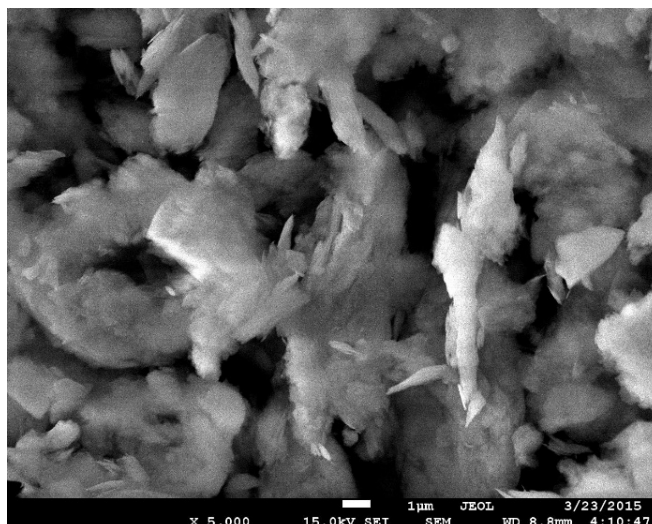


Figure 6.14: The SEM Images of the As-received Talc

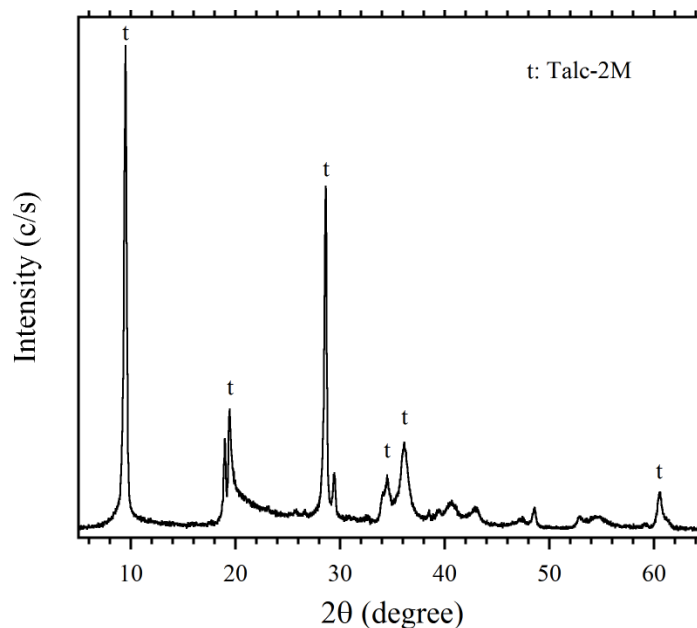


Figure 6.15: The XRD Patterns of the 400°C Calcined Talc

It is possible to state that the hypothesis posed at the beginning is confirmed by the findings indicated here, that is, static water contact angles of samples were found to be in turn 165° and 166° as depicted in Figure 6.16a,b. For the talc surface with grafting density of $10 \mu\text{mol}/\text{m}^2$, the surface resulted in $\theta_{\text{adv}}/\theta_{\text{rec}}=159.25^\circ/138.68^\circ$ ($\text{CAH}\approx 20.57$) by sliding method (Figure 6.17). In addition to high contact angle hysteresis, the water bead was also pinned to the surface at any tilt angle ranging between 0° and 90° . These are considered to stem from the rough surface with

complete wetting between the water bead and surface interface, which may be attributed to Wenzel's model describing homogeneous wetting regime [26, 74].

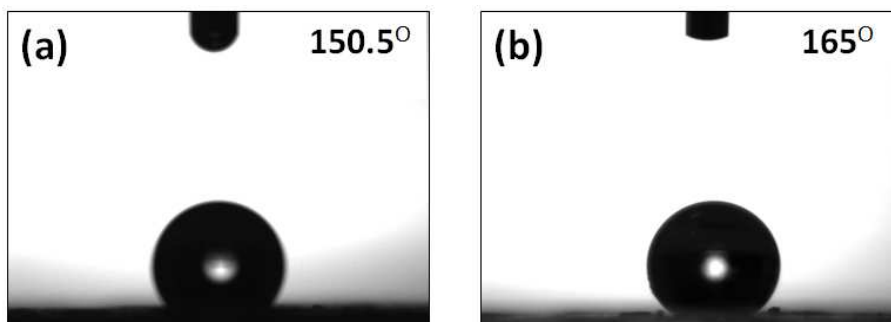


Figure 6.16: Water Contact Angles of PFDec-MCS Modified TALC a) HME-13, b) HME-14

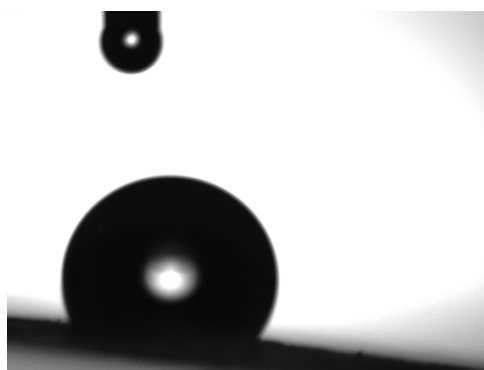


Figure 6.17: Dynamic Contact Angle Measurement of HME-14

7. CONCLUSION

Fluorocarbon-functional silanes were indicated to be the most effective modifiers to attain superhydrophobicity on surfaces of natural texture by comparison to hydrocarbon-functional silanes. In this study perfluorodecyl-1H,1H,2H,2H-dimethylchlorosilane (PFDec-MCS) gives best result in fluorocarbon-functional silanes group. Chemical content of the crude and calcined minerals were investigated via XRF technique. When calcination temperature of DE increase, SiO₂ content is increase but also mean particle size increase that is unwanted situation because it provekes the agglomeration. X-ray diffraction phase analysis of the as-received DE is were done to The broad hump in the vicinity of the crystalline peaks (from 10° to 40°) is typical for DE that indicates an amorphous phase as well as crystalline phases. According to the semi-quantitative analysis, the main structure of DE consists of cristobalite (β -SiO₂), quartz (SiO₂), hypothetical silica (SiO₂), opaline silica (SiO₂•nH₂O), sanidine (KAlSi₃O₈), calcite (CaCO₃), muscovite (KAl₂(AlSi₃O₁₀)(F,OH)₂) and dolomite ((Mg,Ca)(CO₃)₂). According to the XRD analysis, the broad hump in the vicinity of the crystalline peaks (from 10° to 40°) is typical for DE that shows an amorphous phase as well as crystalline phases. The main structure of DE calcined at 400°C consists of hypothetical silica (SiO₂), cristobalite (β -SiO₂), quartz (SiO₂), sanidine (KAlSi₃O₈), calcite (CaCO₃) and dehydroxlated muscovite. Also, opaline silica (SiO₂•nH₂O) is decomposed and the cristobalite peak increase. In the DE calcined at 800°C, calcite peaks disappeared as well as quartz peak increased. The XRD result of DE calcined at 1000°C indicated that the silica structures transformed to cristobalite crystalline phase. Also, anorthoclase (KAlSi₃O₈) and diopside ((Ca,Mg)(Si₂O₆)) crystalline phases occurred in higher temperatures. The covalent attachment of silanes was borne out by XPS method. Water vapor affinity data of surface grafted particles showed that surface silanols were accessible to reach tunable wettability and to optimize grafting methodology. It can also be deduced that the proposed methodology could pave the way to be applied in another natural powder such as talc. According to thermogravimetric analysis, used to investigate grafting density. With increasing grafting density HME-Blank, HME-5, HME-2, HME-4,HME-3 had increasing weight loss 8.20%, 14.64%, 17.29%, 18.45%, 18.92%, respectively. It can be concluded that as the amount of fluoroalkyl grafting density on the particle surface

increased, the amount of percent weight loss in TGA augmented. This phenomenon was also proven by both BET analysis and static contact angle measurements, that is, increase in grafting density gave rise to decrease in the BET “C constant” (lower surface energy) led also to gradual increase in static contact angle. Results showed us that BET C constant’s and contact angle’ of HME-Blank, HME-5, HME-2, HME-4, HME-3 were 146, 35, 25, 24, 21 and 35.5°, 157°, 163°, 165.5°, 166.5° respectively.

Contact angle measurement shows that carbon chain length is important criteria. The longer carbon chain length, the higher contact angle result. Silanes that were used in this thesis to observe the effect of chain length have 2, 4 and 12 carbon in its structure, and their contact angles were 23°, 74° and 160°, respectively. The treatment with monofunctional chlorosilanes was displayed to provide better superhydrophobic feature than multifunctional counter parts. Dynamic contact angle measurements resulted in low contact angle hysteresis and rolling off the water bead even with small droplet volume at very low tilt angle for DE samples. However, as for talc, the water bead was pinned to the surface at any tilt angle ranging between 0° and 90° and caused high contact angle hysteresis. This result is considered to be due to the rough surface with complete wetting between the water droplet and surface interface, which might be related to Wenzel’s model describing homogeneous wetting regime. The study offers important insights into producing superhydrophobic surfaces and potential synergistic approach to be implemented to any proper inherent texture for the production of SH powders.

7.1. Recommendations for Future Works

This section provides recommendations for future work, based on the studying talc that calcined at different temperature. Additionally, recommendations based on unattempted experiments that continue with the different (size, chemical composition etc.) diatomit sample.

8. REFERENCES

1. **Nosonovsky, M. and B. Bhushan**, (2007). *Biomimetic superhydrophobic surfaces: multiscale approach*. Nano letters, **7**(9): p. 2633-2637.
2. **Jung, Y.C. and B. Bhushan**, (2006). *Contact angle, adhesion and friction properties of micro-and nanopatterned polymers for superhydrophobicity*. Nanotechnology, **17**(19): p. 4970.
3. **Neinhuis, C. and W. Barthlott**, (1997). *Characterization and distribution of water-repellent, self-cleaning plant surfaces*. Annals of Botany, **79**(6): p. 667-677.
4. **Koch, K. and H.-J. Ensikat**, (2008). *The hydrophobic coatings of plant surfaces: epicuticular wax crystals and their morphologies, crystallinity and molecular self-assembly*. Micron, **39**(7): p. 759-772.
5. **Campos, R., et al.**, (2011). *Fluoroalkyl-Functionalized Silica Particles: Synthesis, Characterization, and Wetting Characteristics*. Langmuir, **27**(16): p. 10206-10215.
6. **Simpson, J.T. and B.R. D'Urso**, *Superhydrophobic diatomaceous earth*. 2012, Google Patents.
7. **Guo, M., et al.**, (2010). *Amphiphobic Nanofibrous Silica Mats with Flexible and High-Heat-Resistant Properties*. Journal of Physical Chemistry C, **114**(2): p. 916-921.
8. **Kumar, R.T.R., K.B. Mogensen, and P. Boggild**, (2010). *Simple Approach to Superamphiphobic Overhanging Silicon Nanostructures*. Journal of Physical Chemistry C, **114**(7): p. 2936-2940.
9. **Li, H.J., et al.**, (2001). *Super-"amphiphobic" aligned carbon nanotube films*. Angewandte Chemie-International Edition, **40**(9): p. 1743-1746.
10. **Darmanin, T. and F. Guittard**, (2009). *One-pot method for build-up nanoporous super oil-repellent films*. Journal of Colloid and Interface Science, **335**(1): p. 146-149.
11. **Hsieh, C.T., F.L. Wu, and W.Y. Chen**, (2010). *Superhydrophobicity and superoleophobicity from hierarchical silica sphere stacking layers*. Materials Chemistry and Physics, **121**(1-2): p. 14-21.
12. **Oliveira, N.M., R.L. Reis, and J.o.F. Mano**, (2013). *Superhydrophobic surfaces engineered using diatomaceous earth*. ACS applied materials & interfaces, **5**(10): p. 4202-4208.
13. **Roach, P., N.J. Shirtcliffe, and M.I. Newton**, (2008). *Progress in superhydrophobic surface development*. Soft Matter, **4**(2): p. 224-240.
14. **Bhushan, B. and Y.C. Jung**, (2011). *Natural and biomimetic artificial surfaces for superhydrophobicity, self-cleaning, low adhesion, and drag reduction*. Progress in Materials Science, **56**(1): p. 1-108.
15. **Zhang, X., et al.**, (2008). *Superhydrophobic surfaces: from structural control to functional application*. Journal of Materials Chemistry, **18**(6): p. 621-633.
16. **Gao, L., T.J. McCarthy, and X. Zhang**, (2009). *Wetting and Superhydrophobicity†*. Langmuir, **25**(24): p. 14100-14104.
17. **Xin, B. and J. Hao**, (2010). *Reversibly switchable wettability*. Chemical Society Reviews, **39**(2): p. 769-782.
18. **D'Urso, B.R. and J.T. Simpson**, *Superhydrophobic diatomaceous earth*. 2012, Google Patents.

19. **Holmberg, K., et al.**, (2002). *And Polymers In Aqueous Solution*. John Wiley and Sons, West Sussex: p. 108-109.
20. **Ogihara, H., et al.**, (2012). *Simple method for preparing superhydrophobic paper: spray-deposited hydrophobic silica nanoparticle coatings exhibit high water-repellency and transparency*. *Langmuir*, **28**(10): p. 4605-4608.
21. **Young, T.**, (1805). *An essay on the cohesion of fluids*. Philosophical Transactions of the Royal Society of London: p. 65-87.
22. **Yuan, Y. and T.R. Lee**, *Contact angle and wetting properties*, in *Surface science techniques*. 2013, Springer. p. 3-34.
23. **Xia, F. and L. Jiang**, (2008). *Bio-inspired, smart, multiscale interfacial materials*. *Advanced materials*, **20**(15): p. 2842-2858.
24. **Sun, T., et al.**, (2005). *Bioinspired surfaces with special wettability*. *Accounts of Chemical Research*, **38**(8): p. 644-652.
25. **Johnson, R. and R. Dettre**, *Wetting of low-energy surfaces*. 1993, Marcel Dekker: New York.
26. **Marmur, A.**, (2003). *Wetting on hydrophobic rough surfaces: to be heterogeneous or not to be?* *Langmuir*, **19**(20): p. 8343-8348.
27. **Feng, X. and L. Jiang**,(2006). *Design and creation of superwetting/antiwetting surfaces*. *Advanced Materials*, **18**(23): p. 3063-3078.
28. **Quéré, D.**, (2002). *Rough ideas on wetting*. *Physica A: Statistical Mechanics and its Applications*, **313**(1): p. 32-46.
29. **Marmur, A.**, (2004). *The lotus effect: superhydrophobicity and metastability*. *Langmuir*, **20**(9): p. 3517-3519.
30. **Li, D. and A. Neumann**, (1996). *Thermodynamic status of contact angles*. *Surfactant science series*: p. 109-168.
31. **Zhang, X., X. Liu, and G. Meng**, (2005). *Sintering kinetics of porous ceramics from natural diatomite*. *Journal of the American Ceramic Society*, **88**(7): p. 1826-1830.
32. **Akhtar, F., P.O. Vasiliev, and L. Bergström**, (2009). *Hierarchically porous ceramics from diatomite powders by pulsed current processing*. *Journal of the American Ceramic Society*, **92**(2): p. 338-343.
33. **Aderdour, H., et al.** *Diatomite based ceramics macro-and microscopic characterization*. in *Journal de Physique IV (Proceedings)*. 2005. EDP sciences.
34. **Begum, G., et al.**, (2010). *Bioinspired Silicification of Functional Materials: Fluorescent Monodisperse Mesostructure Silica Nanospheres*. *Chemistry of Materials*, **22**(2): p. 551-556.
35. **Fei, B., et al.**, (2007). *Preparation of a panoscopic mimic diatom from a silicon compound*. *Small*, **3**(11): p. 1921-1926.
36. **Oliveira, N.M., R.L. Reis, and J.F. Mano**, (2013). *Superhydrophobic Surfaces Engineered Using Diatomaceous Earth*. *Acs Applied Materials & Interfaces*, **5**(10): p. 4202-4208.
37. **Özen, İ., S. Şimşek, and G. Okyay**, (2015). *Manipulating surface wettability and oil absorbency of diatomite depending on processing and ambient conditions*. *Applied Surface Science*, **332**: p. 22-31.
38. **Taylor, L.**, (2003). *Smooth operator: Talc gets specialised for growth*. *Industrial minerals*, (428): p. 24-33.

39. **Fowkes, F.M. and W.D. Harkins**, (1940). *The state of monolayers adsorbed at the interface solid—aqueous solution*. Journal of the American Chemical Society, **62**(12): p. 3377-3386.
40. **Schrader, M.E. and S. Yariv**, (1990). *Wettability of clay minerals*. Journal of colloid and interface science, **136**(1): p. 85-94.
41. **Giese, R., et al.**, *Proceedings of the 9th International Clay Conference*. 1990. p. 33-41.
42. **Giese, R., P. Costanzo, and C. Van Oss**, (1991). *The surface free energies of talc and pyrophyllite*. Physics and Chemistry of Minerals, **17**(7): p. 611-616.
43. **Norris, J., et al.**,(1993). *The surface energies of cation substituted laponite*. Clay Minerals, **28**: p. 1-1.
44. **Rotenberg, B., A.J. Patel, and D. Chandler**, (2011). *Molecular explanation for why talc surfaces can be both hydrophilic and hydrophobic*. Journal of the American Chemical Society, **133**(50): p. 20521-20527.
45. **Wallqvist, V., et al.**, (2006). *Interaction forces between talc and hydrophobic particles probed by AFM*. Colloids and Surfaces A: Physicochemical and Engineering Aspects, **277**(1): p. 183-190.
46. **Guo, Z., W. Liu, and B.-L. Su**, (2011). *Superhydrophobic surfaces: from natural to biomimetic to functional*. Journal of colloid and interface science, **353**(2): p. 335-355.
47. **Barthlott, W. and C. Neinhuis**, (1997). *Purity of the sacred lotus, or escape from contamination in biological surfaces*. Planta, **202**(1): p. 1-8.
48. **Buszewski, B., et al.**, (1998). *Survey and trends in the preparation of chemically bonded silica phases for liquid chromatographic analysis*. Journal of High Resolution Chromatography, **21**(5): p. 267-281.
49. **Sayari, A. and S. Hamoudi**, (2001). *Periodic mesoporous silica-based organic-inorganic nanocomposite materials*. Chemistry of Materials, **13**(10): p. 3151-3168.
50. **Pickering, J.**, Patent 7,252,885. 2007, Aug.
51. **Coggio, W.**, Patent 7,473,462. 2009, Jan.
52. **Sagiv, J.**, (1980). *Organized monolayers by adsorption. 1. Formation and structure of oleophobic mixed monolayers on solid surfaces*. Journal of the American Chemical Society, **102**(1): p. 92-98.
53. **Fields, J.T., A. Garton, and M.D. Poliks**,(1996). *Fluoroalkylsilanes in silica/fluoropolymer composites*. Polymer composites, **17**(2): p. 242-250.
54. **Berendsen, G.E., et al.**, (1980). *(Heptadecafluorodecyl) dimethylsilyl bonded phase for reversed-phase liquid chromatography*. Analytical Chemistry, **52**(12): p. 1990-1993.
55. **Roshchina, T., et al.**, (2009). *Adsorption of water, diethyl ether, and acetonitrile on silicas with grafted perfluorohexyl coatings*. Russian Journal of Physical Chemistry A, **83**(2): p. 290-297.
56. **Monde, T., et al.**, (1997). *Adsorption characteristics of silica gels treated with fluorinated silylation agents*. Journal of colloid and interface science, **185**(1): p. 111-118.
57. **Gras, S.L., et al.**, (2007). *Intelligent control of surface hydrophobicity*. ChemPhysChem, **8**(14): p. 2036-2050.
58. **Wang, R., et al.**, (1997). *Light-induced amphiphilic surfaces*. Nature, **388**: p. 431-432.

59. **Feng, X., et al.**, (2004). *Reversible super-hydrophobicity to super-hydrophilicity transition of aligned ZnO nanorod films*. Journal of the American Chemical Society, **126**(1): p. 62-63.
60. **Ulman, A.**, (1996). *Formation and structure of self-assembled monolayers*. Chemical reviews, **96**(4): p. 1533-1554.
61. **Rye, R., G. Nelson, and M. Dugger**, (1997). *Mechanistic aspects of alkylchlorosilane coupling reactions*. Langmuir, **13**(11): p. 2965-2972.
62. **McGovern, M.E., K.M. Kallury, and M. Thompson**, (1994). *Role of solvent on the silanization of glass with octadecyltrichlorosilane*. Langmuir, **10**(10): p. 3607-3614.
63. **Aswal, D., et al.**, (2006). *Self assembled monolayers on silicon for molecular electronics*. Analytica chimica acta, **568**(1): p. 84-108.
64. **Moon, J.H., et al.**, (1996). *Formation of uniform aminosilane thin layers: an imine formation to measure relative surface density of the amine group*. Langmuir, **12**(20): p. 4621-4624.
65. **Moon, J.H., et al.**, (1997). *Absolute surface density of the amine group of the aminosilylated thin layers: ultraviolet-visible spectroscopy, second harmonic generation, and synchrotron-radiation photoelectron spectroscopy study*. Langmuir, **13**(16): p. 4305-4310.
66. **Bierbaum, K., et al.**, (1995). *A near edge X-ray absorption fine structure spectroscopy and X-ray photoelectron spectroscopy study of the film properties of self-assembled monolayers of organosilanes on oxidized Si (100)*. Langmuir, **11**(2): p. 512-518.
67. **Wasserman, S.R., Y.T. Tao, and G.M. Whitesides**, (1989). *Structure and reactivity of alkylsiloxane monolayers formed by reaction of alkyltrichlorosilanes on silicon substrates*. Langmuir, **5**(4): p. 1074-1087.
68. **Greenwood, P.**, *Surface modifications and applications of aqueous silica sols*. 2010, Chalmers University of Technology.
69. **Liu, L., et al.**, (2009). *Humidity sensitivity of multi-walled carbon nanotube networks deposited by dielectrophoresis*. Sensors, **9**(3): p. 1714-1721.
70. **Kazakevich, Y.V. and A.Y. Fadeev**, (2002). *Adsorption characterization of oligo (dimethylsiloxane)-modified silicas: an example of highly hydrophobic surfaces with non-aliphatic architecture*. Langmuir, **18**(8): p. 3117-3122.
71. **Nikoobakht, B. and M.A. El-Sayed**, (2001). *Evidence for bilayer assembly of cationic surfactants on the surface of gold nanorods*. Langmuir, **17**(20): p. 6368-6374.
72. **Wang, Q., et al.**, (2006). *Surface confined ionic liquid as a stationary phase for HPLC*. Analyst, **131**(9): p. 1000-1005.
73. **Thomas, M.M. and J.A. Clouse**, (1989). *Thermal analysis of compounds adsorbed on low-surface-area solids: Part 1. measurement and characterization by TGA*. Thermochemica acta, **140**: p. 245-251.
74. **Ebert, D. and B. Bhushan**, (2012). *Transparent, superhydrophobic, and wear-resistant coatings on glass and polymer substrates using SiO₂, ZnO, and ITO nanoparticles*. Langmuir, **28**(31): p. 11391-11399.
75. **Gao, L. and T.J. McCarthy**, (2007). *Ionic liquid marbles*. Langmuir, **23**(21): p. 10445-10447.
76. **Aussillous, P. and D. Quéré**, (2001). *Liquid marbles*. Nature, **411**(6840): p. 924-927.

77. **Tripp, C., R. Veregin, and M. Hair**, (1993). *Effect of fluoroalkyl substituents on the reaction of alkylchlorosilanes with silica surfaces*. *Langmuir*, **9**(12): p. 3518-3522.
78. **Fadeev, A.Y. and T.J. McCarthy**, (2000). *Self-assembly is not the only reaction possible between alkyltrichlorosilanes and surfaces: monomolecular and oligomeric covalently attached layers of dichloro- and trichloroalkylsilanes on silicon*. *Langmuir*, **16**(18): p. 7268-7274.
79. **Hair, M. and C. Tripp**, (1995). *Alkylchlorosilane reactions at the silica surface*. *Colloids and Surfaces A: Physicochemical and Engineering Aspects*, **105**(1): p. 95-103.
80. **Blitz, J.P., R.S. Murthy, and D.E. Leyden**, (1988). *Studies of silylation of Cab-O-Sil with methoxymethylsilanes by diffuse reflectance FTIR spectroscopy*. *Journal of colloid and interface science*, **121**(1): p. 63-69.
81. **Xu, B. and N. Vermeulen**, (1988). *Preparation of wall-coated open-tubular capillary columns for gas chromatography*. *Journal of Chromatography A*, **445**: p. 1-28.
82. **Houde, M., et al.**, (2006). *Biological monitoring of polyfluoroalkyl substances: a review*. *Environmental science & technology*, **40**(11): p. 3463-3473.
83. **Kudo, N. and Y. Kawashima**, (2003). *Toxicity and toxicokinetics of perfluorooctanoic acid in humans and animals*. *The Journal of toxicological sciences*, **28**(2): p. 49-57.
84. **Giesy, J.P. and K. Kannan**, (2001). *Global distribution of perfluorooctane sulfonate in wildlife*. *Environmental science & technology*, **35**(7): p. 1339-1342.
85. **Darmanin, T., et al.**, (2010). *Hydrocarbon versus fluorocarbon in the electrodeposition of superhydrophobic polymer films*. *Langmuir*, **26**(22): p. 17596-17602.
86. **Balek, V., et al.**, (2008). *Thermal behavior of ground talc mineral*. *Journal of Mining and Metallurgy, Section B: Metallurgy*, **44**(1): p. 7-17.

URL-1 <http://www.deutschesmuseum.de/en/exhibitions/newtechnologies/>

URL-2 <https://www.nextnature.net/2012/12/nanotech-diatoms/>

URL-3 <http://2012.extrememarine.org.uk/diatoms/diatoms/index.html>

URL-4 <http://mvascientificconsultants.com/>

CURRICULUM VITAE

Name Surname: Hande ALPTEKİN

Place and Date of Birth: Izmir / 1989

E-Mail: hndalptekin@gmail.com

B.Sc.: EgeUniversity, Faculty of Engineering, Chemical Engineering

PUBLICATIONS/PRESENTATIONS ON THE THESIS

1. Alptekin H., Arkan E., Ozbek C., Can M., Farzaneh A., Sutcu M., Okur S. Surface modification, characterization and tunable superhydrophobicity of natural minerals. (Submitted to Journal)
2. H. Alptekin, E. Arkan, C. Özbek, M. Can, A. Farzaneh, M. Sütçü, S. Okur, B. Sağlam, Investigation of Tunable Wetting Properties of Modified Natural Mineral Powders, International Porous and Powder Materials Symposium, 15-18 September, İzmir/TURKEY (oral presentation)